REFERENCES

[1] T. S. Rappaport, “Wireless Communications - Principles and Practice”, Second Edition, Prentice-Hall, 2002

[2] http://www.gsmworld.com

[3] S. M. Alamouti, "A simple transmitter diversity scheme for wireless communications," *IEEE J. Select. Area Commun.*, vol. 16, pp. 1451-1458, Oct. 1998.

[4] J. Korhonen, “Introduction to 3G Mobile Communications, Second Edition”, Artech House, 2003

[5] K. Feher, “Wireless Digital Communications -Modulation and Spread Spectrum Applications”, 1st Edition, Prentice-Hall, 1995.

[6] J. G. Proakis, “Digital Communications, 4th Edition”, McGraw-Hill, 2001.

[7] S. Haykin, “*Communication systems*”, John Wiley and Sons, New York, 1994

[8] D. Rajan and S.D. Gray, “Transmit Diversity Schemes for CDMA-2000,” *IEEE Conf. On Wireless Commun. And Networking* (*WCNC1999)*, vol.2, pp. 669 – 673, New Orleans, Los Angles, September 1999.

[9] R. Katulski and M. Mikolajski, “Transmit Diversity in Mobile Communications,” *Int. Conf. On Microwaves, Radar and Wireless Commun.* (*MIKON2002)*, vol.3, pp. 878 – 881.

[10] D. Gerlach and P. Paulraj, "Adaptive Transmitting Antenna Arrays with Feedback," *IEEE Sig. Proc. Lett.*, vol. 1, no.10, pp. 150-152, October 1994.

[11] R. Price and P. E. Green, “A Communication Technique for Multipath Channels,” *Proc. IRE*, vol.46, pp. 555–570, March 1958.

[12] G.D. Forney, (1966), “Concatenated Codes”, Cambridge MA: MIT Press.

[13] C. Berrou, A. Glavieux and P. Thitimajshima, “Near Shannon Limit Error Correction Coding and Decoding: Turbo codes,” *IEEE Int. Conf. Commun.*, Geneva, Switzerland, pp. 1064 - 1070, May 1993.

[14] J. L. Massey, “Step-by-Step Decoding of BCH codes,” *IEEE Trans. Inform. Theory*, vol. IT-11, pp. 580 – 585, October 1965.

[15] L. Staphorst and L. P. Linde, “Performance evaluation of Viterbi Decoded Reed-Solomon Block Codes in Additive White Gaussian Noise and Flat Fading Channel Conditions”, *IEEE Conf. On Wireless Commun. And Networking (WCNC2002)*, Orlando, Florida, March 2002.

[16] J.C. Guey, M.P. Fitz, M.R. Bell and W.Y. Kuo, "Signal design for transmitter diversity wireless communication systems over Rayleigh fading channels," in *VTC’96: Vehicular Technology Conference*, pp. 136-140, 1996.

[17] L. Staphorst, “Viterbi Decoded Linear Block Codes for Narrowband and Wideband Wireless Communication Over Mobile Fading Channels”, M.Eng dissertation, University of Pretoria, July 2005.

[18] C.B. Papadias and G.J. Foschini, “Capacity Approaching Space-Time Codes for Systems Employing Four Transmitter Antennas,” *IEEE Trans. Inform. Theory*, vol.49, No.3, March 2003.

[19] L. Staphorst, F. Maasdorp and L.P. Linde, "Simulation Study of a Space-Sequence Transmit Diversity Scheme for DS/SSMA Systems (Part I)," *ICT 2005 Cape Town RSA*, May 2005.

[20] L. Staphorst, F. Maasdorp and L.P. Linde, "Simulation Study of a Space-Sequence Transmit Diversity Scheme for DS/SSMA Systems (Part II)," *ICT 2005 Cape Town RSA*, May 2005.

[21] F. Maasdorp, L. Staphorst and L.P. Linde, "A Full Rate, Full Diversity Space-Time Block Code for an Arbitrary number of Transmit Antennas". Submitted to *IEEE Trans. Veh. Tech.*

[22] V. Tarokh, N. Seshadri, and A. R. Calderbank, "Space-time Block codes from orthogonal designs," *IEEE Trans. Inform. Theory*, vol. 45, no.5, pp. 1456-1467, July 1999.

[23] E. Biglieri, G. Taricco and A. Tulino, "Performance of Space-time Codes for a Large Number of Antennas," *IEEE Trans. Inform. Theory*, vol. 48, no.7, pp. 1794-1803, July 2002.

[24] C. Gao, A. M. Haimovich and D. Lao, "BER Analysis of MPSK Space-Time Block Codes," *IEEE Commun. Lett.*, vol.7, pp. 314 – 316, July 2003.

[25] V. Tarokh, N. Seshadri, and A. R. Calderbank, "Space-time block coding for wireless communications: Performance Results," *IEEE J. Select. Areas Commun.*, vol. 17, no.3, pp. 451-460, March 1999.

[26] G.J. Foschini and M.J. Gans, "On Limits of Wireless Communications in a Fading Environment When using Multiple Antennas," *Wireless Pers. Commun.*, vol. 6, pp. 311-315, 1998.

[27] I.E. Teletar, "Capacity of Multi-Antenna Gausssian Channels," *Euro. Trans. Telecommun.*, vol. 10, no. 6, pp. 585-595, Nov. 1999.

[28] R. Doostnejad, T. J. Lim and E. Sousa, "Transmitter and Receiver Designs for the MIMO Fading Broadcast Channel," Department of ECE, University of Toronto.

[29] C. E. Shannon, "A Mathematical Theory of Communication", *Bell Systems Technical Journal*, vol. 27, pp.379 – 423 and 623 – 656, 1948.

[30] J. Winters, J. Salz and R. D. Gitlin, "The impact of antenna diversity on the capacity of wireless communication systems," *IEEE Trans. Commun.*, vol. 42. no.2/3/4, pp. 1740-1751, Feb./Mar./Apr. 1994.

[31] T. Marzetta and B. Hochwald, "Capacity of a mobile multiple antenna communication link in Rayleigh flat fading," *IEEE Trans. Inform. Theory*, vol. 45, pp. 139 -158, January 1999.

[32] V. Tarokh, N. Seshadri and A. R. Calderbank, "Space-time codes for high data rate wireless communication: Performance analysis and code construction," *IEEE Trans. Inform. Theory*, vol. 44, no.2, pp. 744-765, March 1998.

[33] A. R. Hammons and H. E. Gamal, "On the theory of space-time codes for PSK modulation," *IEEE Trans. Inform. Theory*, vol. 46, pp.524-542, March 2002.

[34] S. Baro, G. Bauch and A. Hansman, "Improved codes for space-time trellis codes modulation," *IEEE Commun. Lett.*, pp. 20-22, Jan. 2000.

[35] O. Tirkkonen and A. Hottinen, "Complex space-time block codes for four Tx antennas," in *GLOBECOM Conf. Records*, vol. 2, pp. 1005-1009, San Francisco, CA, Nov.-Dec. 2000.

[36] L. A. Dalton and C. N. Georghiades, "A Four Transmit Antenna Orthogonal Space-Time Code with Full Diversity and Rate," in *Proc. 40th Annual Allerton Conf. On Commun. Control, and Computing*, Monticello, IL, October 2002.

[37] M. M. da Silva and A. Correia, "Space-Time Coding schemes for 4 or more Antennas," *Proceedings of IEEE PIMRC 2002*, Lisbon, Portugal, September 2002.

[38] B. M. Hochwald and T.L. Marzetta, "Unitary space-time modulation for multiple-antenna communication in Rayleigh flat fading", *IEEE Trans. Inform. Theory*, vol 46, pp. 543-564, March 2000.

[39] B. M. Hochwald and W. Sweldens, "Differential unitary space-time modulation," *IEEE Trans. Commun.*, vol. 48, pp. 2041-2052, December 2000.

[40] O. Tirkkonen, A. Boariu and A. Hottinen, "Minimal non-orthogonality rate 1 space-time block code for 3+ Tx," in *IEEE Int. Symposium on Spread Spectrum Techniques & Applications*, pp.429-432, New Jersey, USA, September 2000.

[41] H. Jafarkhani, "A quasi-orthogonal space-time block code," *IEEE Trans. Commun.*, vol. 49, pp. 1-4, January 2001.

[42] A. Yongacoglu and M. Siala, "Performance of diversity systems with 2 and 4 transmit antennas," in *Proceedings Int. Conf Commun. Tech. (WCC-ICCT)*, pp. 148-150, Peking, China, 2000.

[43] L. M. A Jalloul, K. Rohani, K. Kuchi and J. Chen, "Performance analysis of CDMA transmit diversity methods," in *Proc. IEEE Vehicular Tech. Conf. (VTC)*, vol. 3, pp. 1326-1330, Amsterdam, Netherlands, October 1999.

[44] S. Rouquette, S. Merigeault and K. Gosse, "Orthogonal full diversity Space-Time block coding based on transmit channel state information for 4 Tx antennas," in *Proc. IEEE Int. Conf. Commun. (ICC)*, vol. 1, pp. 558-562, New York City, NY, April-May 2002.

[45] M. O. Damen, K. Abed-Meraim and J. C. Belfiore, "Transmit diversity using rotated constellations with Hadamard transform," in *Proc. Adaptive Systems for Signal Processing, Commun. And Control Conf.*, pp. 396-401, Lake Louise, Alberta, Canada, October 2000.

[46] Y. Xin, Z. Wang and G. B. Giannakis, "Space-time diversity systems based on unitary constellation-rotating precoders," in *Proc. IEEE Int. Conf. Acoust.,Speech, Signal Processing (ICASSP)*, pp. 2429-2432, Salt Lake City, Utah, May 2001.

[47] V. M. DaSilva and E. S. Sousa, "Fading-resistant modulation using several transmitter antennas," *IEEE Trans. Commun.*,vol. 45, pp. 1236-1244, October 1997.

[48] H. El Gamal and A.R. Hammons, "On the design and performance of Algebraic Space-Time Codes for BPSK and QPSK Modulation," *IEEE Trans. Commun.*, vol. 50. no.6, pp. 907-913, June 2002.

[49] V. Tarokh and H. Jafarkhani, "A Differential Detection Scheme for Transmit Diversity," *IEEE J. Select. Areas Commun.*, vol. 18, no.7, pp. 1169-1174, July 2000.

[50] Y. Li, C.N. Georghiades and G. Huang, "Iterative Maximum-Likelihood Sequence Estimation for Space-Time Coded Systems," *IEEE Trans. Commun.*, vol. 49. no.6, pp. 948-951, June 2001.

[51] J.D. Terry and J.T. Heiskala, "Spherical Space-Time Codes (SSTC)," *IEEE Commun. Lett.*, vol.5, no.3, pp. 107-109 , March 2001.

[52] M.O. Damen, A. Tewfik and J. Belfiore, "A Construction of a Space-Time Code Based on Number Theory," *IEEE Trans. Inform. Theory*, vol. 48, no.3, pp. 753-760, March 2002.

[53] E.G. Larsson, P. Stoica and J. Li, "On Maximum-Likelihood Detection and Decoding for Space-Time Coding Systems," *IEEE Trans. Signal Processing*, vol. 50, no.4, pp. 937-944, April 2002.

[54] R. Gold, "Optimal Binary Sequences for Spread Spectrum Multiplexing," *IEEE Trans. Inform. Theory*, vol. IT-13, pp. 619–621, October 1967.

[55] M. P. Lötter and L.P. Linde, "Constant Envelope Filtering of Complex Spreading Sequences," *IEE Electronic Letters*, vol. 31, no. 17, pp. 1406 – 1407, August 1995.

[56] M. P. Lötter and L.P. Linde, "A Class of Bandlimited Complex Spreading Sequences with Analytic Properties," in *Proc. IEEE Int. Symp. on Spread Spectrum Techniques and Applications*, (Mainz, Germany), pp. 662 – 666, 22 – 25 September 1996.

[57] B. M. Popovic, "Generalised Chirp Like Polyphase Sequences with Optimum Correlation Properties," *IEEE Trans. Inform. Theory*, vol. 38, July 1992.

[58] M. Jamil, L. P. Linde, J. E. Cilliers, and D. J. van Wyk, "Comparison of Complex Spreading Sequences Based on Filtering Methods and Mean Square Correlation Characteristics," *Transactions of the SAIEE*, vol. 89, no. 3, pp. 98–112, September 1998.

[59] R. L. Frank and S. A. Zadoff, "Phase Shift Pulse Codes with Good Periodic Correlation Properties," *IRE Transactions on Information Theory*, vol. IT-7, pp. 381–382, October 1962.

[60] S. M. Korne and D. V. Sarwate, "Quadriphase Sequences for Spread Spectrum Multiple Access Communication," *IEEE Trans. Inform. Theory*, vol. IT-38, no. 3, pp. 1101 – 1113, May 1992.

[61] M. Jamil, "Comparative Study of Complex Spreading Sequences for CDMA Applications," Master's thesis, University of Pretoria, May 1999.

[62] M. P. Lötter, “A Generalised Linear Root-of-Unity Interpolation Filter,” in *Proc. IEEE COM-SIG’95s*, (University of Pretoria, Pretoria, South Africa), pp. 43 – 46, September 1995.

[63] S. Haykin and M. Moher, “Modern Wireless Communications”, Prentice-Hall, 2005.

[64] J. G. Proakis, “Contemporary Communication Systems using Matlab”, Brooks/Cole, 2000.

[65] B. Hochwald, T.L. Marzetta and C.B. Papadias, "A Transmitter Diversity Scheme for Wideband CDMA systems based on Space-Time Spreading," *IEEE J. Select. Areas Commun.*, vol. 19, no.1, pp. 48-60, January 2001.

[66] H. Huang, H. Viswanathan and G. J. Foschini, "Multiple Antennas in cellular CDMA systems: transmission, detection and spectral efficiency," *IEEE Trans. Wireless Commun.*, vol. 1, no. 3, pp. 383-392, July. 2002.

[67] J. Wang and K. Yao, "Space-Time Coded Wideband CDMA Systems," *In Proc. IEEE Veh. Tech. Conf. (VTC)*, vol.1, pp. 260 – 264, 2002.

[68] TIA/EIA IS-2000 Physical Layer Specification for CDMA Spread Spectrum Communication System, June 2000.

[69] J. Hamalainen and R. Wichman, “Closed-Loop Transmit Diversity for FDD WCDMA Systems,” Signals, *Systems and Computers 2000*, vol.1, p111-115, Nov.2000.

[70] D.J. van Wyk, P.G.W. van Rooyen and L.P. Linde, “Super-Orthogonal Space-time Turbo Transmit Diversity for CDMA”, *EURASIP Journal on Applied Signal Processing*, vol. 2005, no. 6, pp.861 – 871, January 2005.

[71] D. Gesbert, M. Shafi, D. Shiu, P.J. Smith and A. Naguib, "From Theory to Practice: An Overview of MIMO Space-Time Coded Wireless Systems", *IEEE J. Select. Areas Commun.*, vol. 21, no.3, pp. 281-302, April 2003.

[72] J.K.Cavers, “An analysis of pilot symbol assisted modulation for Rayleigh fading channels”, *IEEE Trans. Veh. Technol.*, vol. 40, pp.686 – 693, Nov. 1991.

[73] B. Raghothaman, R.T. Derryberry and G. Mandyam, “Transmit adaptive array without user-specific Pilot for 3G CDMA,” *IEEE Int. Conference on Acoustics, Speech and Signal processing (ICASSP 2000)*, vol.5, pp.3009-3012, Istanbul, Turkey, June 2000.

[74] W. C. Jakes Jr., "*Microwave Mobile Communications*", Wiley-Interscience, 1974.

[75] R.H. Clarke, "A Statistical Theory of Mobile-Radio reception", *Bell Systems Technical Journal*, vol. 47, pp 957 – 1000, 1968.

APPENDIX A

MAXIMAL - RATIO RECEIVE COMBINING

A.1 APPENDIX OVERVIEW

Until recently, diversity has been obtained by transmission from a single antenna to multiple receive antennas. This method is known as receive diversity and is achieved by a scheme known as MRRC, shown in *Figure A.1*. MRRC is presented in the remainder of *Appendix A.*

A.2 MAXIMAL - RATIO RECEIVE COMBINING

At a given time, a signal s_0 is sent from the transmitter. The channel, which undergoes Rayleigh fading may in the worst case be modelled by a complex multiplicative distortion composed of a magnitude response and a phase response. As shown in *Figure A.1*, h_0 denotes the channel between the transmit antenna and receive antenna zero and h_1 denotes the channel between the transmit antenna and receive antenna one, where

$$h_0 = \alpha_0 \exp(j\vartheta_0)$$
$$h_1 = \alpha_1 \exp(j\vartheta_1) \qquad \text{(A.1)}$$

If noise is added at the two receivers, the resulting received baseband signals are

$$r_0 = h_0 s_0 + n_0$$
$$r_1 = h_1 s_1 + n_1 \qquad \text{(A.2)}$$

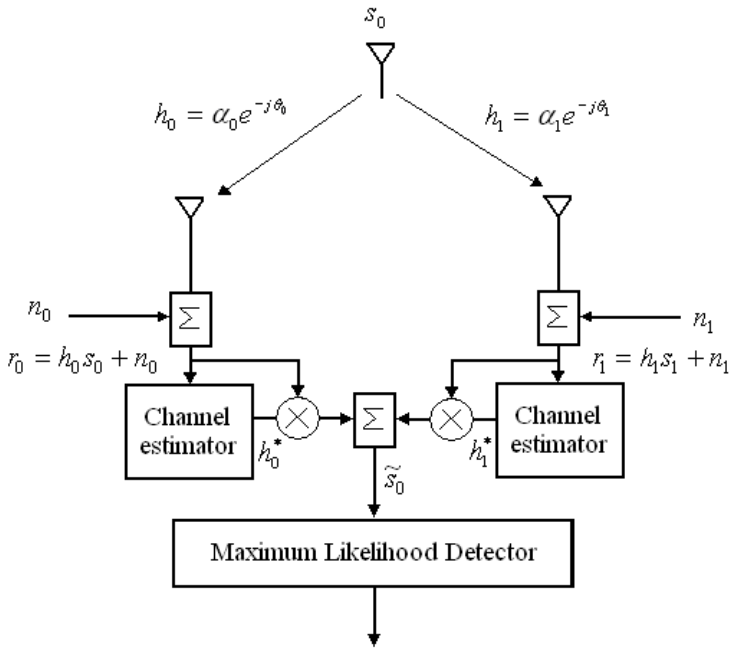

Figure A.1. Receive diversity obtained by two-branch MRRC, taken from [3].

where n_0 and n_1 represent complex Gaussian distributed noise. Because n_0 and n_1 are Gaussian distributed and given that s_0 and s_1 are equiprobable, the ML decision rule applies and the receiver chooses signal s_i, if and only if

$$d^2(r_0, h_0 s_i) + d^2(r_1, h_1 s_i) \le d^2(r_0, h_0 s_k) + d^2(r_0, h_0 s_k) \qquad \forall\, i \ne k \qquad \text{(A.3)}$$

where $d^2(x, y)$ is the squared Euclidean distance between signals x and y, calculated using *Equation (A.4)*

$$d^2(x,y) = (x-y)(x^*-y^*) \tag{A.4}$$

As shown in *Figure A.1*, the receiver's combining scheme for two-branch MRRC are given by *Equation (A.5)*:

$$\begin{aligned}\tilde{s}_0 &= h_0^* r_0 + h_1^* r_1 \\ &= h_0^*(h_0 s_0 + n_0) + h_1^*(h_1 s_0 + n_1) \\ &= (\alpha_0^2 + \alpha_1^2)s_0 + h_0^* n_0 + h_1^* n_1\end{aligned} \tag{A.5}$$

Expanding *Equation (A.3)* and using *Equations (A.4)* and *(A.5)*, *Equation (A.6)* is obtained, stating that: choose s_i if

$$(\alpha_0^2 + \alpha_1^2)|s_i|^2 - \tilde{s}_0 s_i^* - \tilde{s}_0^* s_i \le (\alpha_0^2 + \alpha_1^2)|s_k|^2 - \tilde{s}_0 s_k^* - \tilde{s}_0^* s_k \qquad \forall i \ne k \tag{A.6}$$

is met, or equivalently

$$(\alpha_0^2 + \alpha_1^2 - 1)|s_i|^2 + d^2(\tilde{s}_0, s_i) \le (\alpha_0^2 + \alpha_1^2 - 1)|s_k|^2 + d^2(\tilde{s}_0, s_k) \qquad \forall i \ne k \tag{A.7}$$

For PSK signals the energy in the constellation points are all equal, i.e.:

$$|s_i|^2 = |s_k|^2 = E_s \qquad \forall\, i,k \tag{A.8}$$

Thus, *Equation (A.7)* reduces to *Equation (A.9)* for PSK constellation signals: Choose s_i if

$$d^2(\tilde{s}_0, s_i) \le d^2(\tilde{s}_0, s_k) \qquad \forall i \ne k \tag{A.9}$$

Equation (A.9) is a joint probability function that seeks to minimize the Euclidean distance between the received signal and the constellation points. The ML detector in *Figure A.1* uses the decision rule in *Equation (A.9)* to obtain the optimal solution for $\hat{s}_0$, which is a ML estimate of s_0.

APPENDIX B

ALAMOUTI SPACE – TIME BLOCK CODING

B.1 APPENDIX OVERVIEW

In *Appendix B*, a transmit diversity scheme in baseband, originally proposed by Alamouti [3], is presented and shown in *Figure B.1*.

Appendix B is structured as follows: In *Sections B.2* to *B.4* the main functions of *Figure B.1* are decribed, i.e:

- Encoding and transmission of symbols at the transmitter,
- combing scheme at the receiver,
- decision rule for ML detection.

In *Section B.5* the error performance of the scheme is presented and compared to MRRC. Lastly, some implementation issues are highlighted and discussed in *Section B.6*.

B.2 ENCODING AND TRANSMISSION

With reference to *Figure B.1*, assume that at time *t*, two symbols s_0 and s_1, are simultaneously transmitted from antennas zero and one. At the next symbol period, $t + T$, $-s_1^*$ and s_0^* are transmitted from antennas zero and one, respectively. Thus, encoding is done in both time and space, and is known as space-time coding. The channel can be modelled as described in *Chapter 4*. Assuming that the fading is constant across two consecutive symbols, h_0 and h_1 can be written as

$$\begin{aligned} h_0(t) &= h_0(t+T) = h_0 = \alpha_0 \exp(j\vartheta_0) \\ h_1(t) &= h_1(t+T) = h_1 = \alpha_1 \exp(j\vartheta_1) \end{aligned} \qquad \text{(B.1)}$$

where *T* denotes the symbol duration.

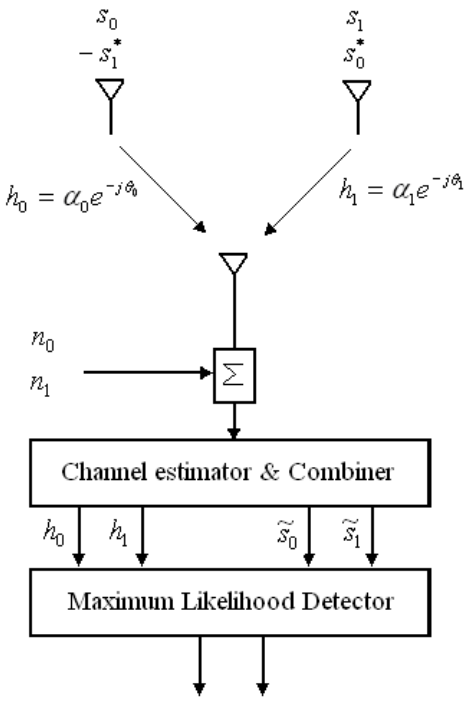

Figure B.1. Two branch transmit diversity with a single receiver, taken from [3].

It follows that the received signal at the receiver can be written as

$$r_0 = r(t) = h_0 s_0 + h_1 s_1 + \eta_0$$
$$r_1 = r(t+T) = -h_0 s_1^* + h_1 s_0^* + \eta_1 \qquad \text{(B.2)}$$

where r_0 and r_1 are the received signals at time t and $t+T$, respectively. These received signals are corrupted by receiver noise, denoted by η_0 and η_1 respectively.

B.3 COMBINING SCHEME

The combiner, as shown in *Figure B.1*, combines the following two signals, which are then passed on to the ML detector:

$$\tilde{s}_0 = h_0^* r_0 + h_1 r_1^*$$
$$\tilde{s}_1 = h_1^* r_0 - h_0 r_1^* \qquad \text{(B.3)}$$

Also note that *Equation (B.3)* differs from *Equation (A.5)*. Substituting *Equations (B.1)* and *(B.2)* into *Equation (B.3)*, *Equation (B.4)* is obtained.

$$\tilde{s}_0 = \left(\alpha_0^2 + \alpha_1^2\right) s_0 + h_0^* \eta_0 + h_1 \eta_1^*$$
$$\tilde{s}_1 = \left(\alpha_0^2 + \alpha_1^2\right) s_1 - h_0 \eta_1^* + h_1^* \eta_0 \qquad \text{(B.4)}$$

B.4 MAXIMUM LIKELIHOOD DETECTION

Using *Equation (A.8)* for $\tilde{s}_0$ and $\tilde{s}_1$, as defined in *Equation (B.4)*, the estimates for $\hat{s}_0$ and $\hat{s}_1$ can be obtained.

It should be noted that the resulting combined signal in *Equation (B.4)* is equivalent to the result in *Equation (A.5)* for MRRC. The only difference is the phase rotations on the noise

components, which do not degrade the effective SNR. Thus, the resulting diversity order of two is similar to the two branch MRRC. It was also shown by Alamouti [3] that the scheme can be extended to two transmit antennas and multiple receive antennas. Using M receive antennas, a diversity order of $2M$ can be obtained. In this dissertation only one receive antenna will be considered.

B.5 ERROR PERFORMANCE

With the performance evaluation of the scheme, the following assumptions are made:

- The total transmit power from the two antennas equals that of a single transmit antenna from the MRRC scheme.
- The amplitude of the fading from each transmit antenna to each receive antenna are mutually uncorrelated and Rayleigh distributed. However, the average signal power from each transmit antenna to each receive antenna are the same.
- Perfect CSI is assumed.

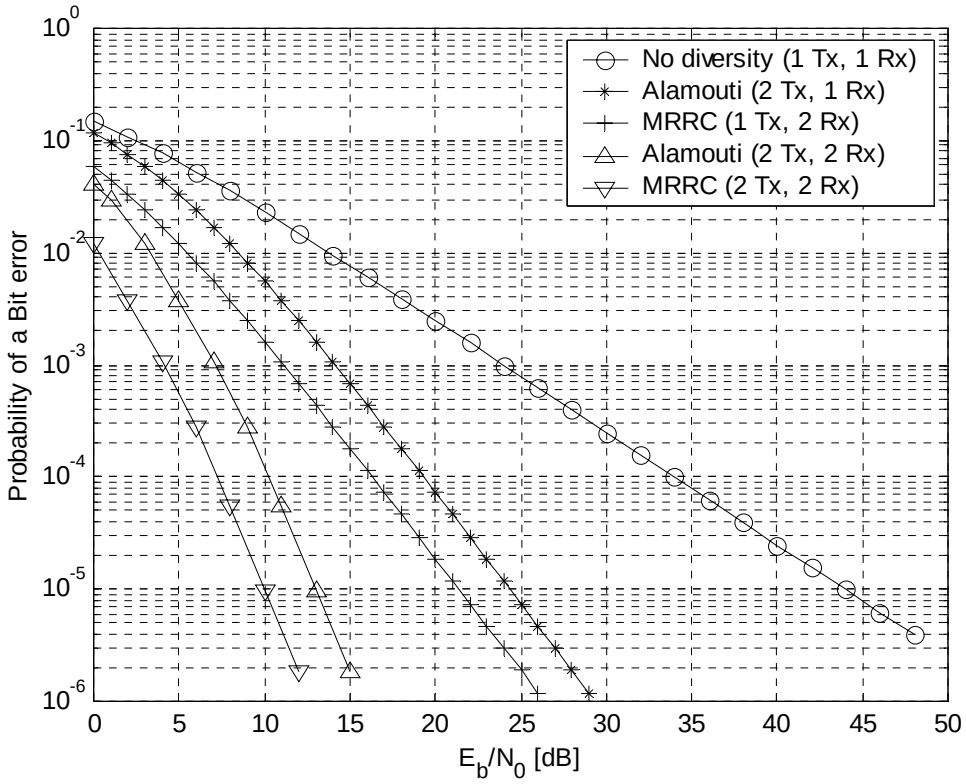

Figure B.2 BER performance of uncoded coherent BPSK for MRRC and the transmit diversity scheme in a Rayleigh fading channel [3].

These assumptions are the basis for comparing this scheme to other schemes. As seen in *Figure B.2*, the transmit diversity scheme performs similar to MRRC with the same number of antennas (see *Section B.6.1* for 3dB performance difference).

B.6 IMPLEMENTATION ISSUES

This section is concerned with the differences observed between the transmit diversity scheme and the MRRC scheme.

B.6.1 Power considerations

As seen in *Figure B.2*, the transmit diversity scheme has a 3dB penalty in SNR performance when compared to the MRRC scheme, due to the transmission of 2 symbols from two different antennas. Thus, only half the power is available to each antenna. This, however, can be a cheaper implementation, due to smaller amplifiers that need to be used.

B.6.2 Sensitivity to channel estimation errors

One method to perform channel estimation is by means of pilot insertion and extraction [72]. This is done by periodically transmitting known symbols to the receiver that are interpolated at the receiver to construct an estimate of the channel. It is interesting to note that the channel estimation error is minimized when the pilot insertion frequency is greater or equal to the channel Nyquist sampling rate. If this condition applies, the errors due to the channel estimation imperfections are minimized.

It should also be noted that twice the number of pilot symbols are added to the transmit diversity scheme, because of the extra antenna present (these pilot symbols should be orthogonal).

B.6.3 Delay effects

The delay for a 2-branch diversity scheme would be 2 symbol periods, where MRRC is only one symbol period. However, if the symbols were sent at the same time on different carriers, the symbol period would also be one.

B.6.4 Antenna Configuration

A primary requirement for diversity improvement is that the signals transmitted from different antennas should be sufficiently decorrelated (less than 70% correlation) and have almost equal gain. To satisfy this requirement, the antennas at the BS should be separated by at least 10λ, and 3λ at the MS [1, 3, 72]. This separation requirement depends on many factors such as antenna height and the scattering environment. It should also be stated that these figures apply mostly to macrocell, urban and suburban environments with relatively large base station antenna heights.

Accordingly, transmit diversity and receive diversity can both be accomplished, or only transmit diversity in the down link and receive diversity in the uplink, assuming the mobile has only a single antenna and the base station consists of multiple antennas.

B.6.5 Soft failure

Receive diversity enables a communication system to still receive a signal if one of the transmission chains fail, but with inferior quality because of the loss of diversity gain. This is called soft failure. This is also accomplished by transmit diversity. For example, suppose $h_1 = 0$ in *Equation (B.2)*, the received signal becomes:

$$r_0 = r(t) = h_0 s_0 + \eta_0$$
$$r_1 = r(t+T) = -h_0 s_1^* + \eta_1 \qquad \text{(B.6)}$$

Thus, the combiner combines the following two estimates:

$$\tilde{s}_0 = h_0^* \left(h_0 s_0 + \eta_0 \right) = \alpha_0^2 s_0 + h_0^* \eta_0$$

$$\tilde{s}_1 = -h_0 \left(-h_0^* s_1 + \eta_1 \right) = \alpha_0^2 s_1 - h_0 \eta_1^* \qquad \text{(B.7)}$$

which is similar to using no diversity at all.

B.6.6 Impact on Interference

The level of interference experienced by the transmit diversity scheme is twice as much as with the MRRC scheme. This interference can be minimized by incorporating techniques such as array processing [1, 5, 6, 7], etc.

APPENDIX C

MOBILE FADING CHANNEL THEORY AND SIMULATIONS

C.1 APPENDIX OVERVIEW

In Appendix C, a summary of multipath fading signal propagation effects contained within the simulation platform and used to generate the proposed DSSTS as well as SSTD scheme's simulation results, is presented. This Appendix is structured as follows: In *Section C.2* a general overview of small-scale multipath fading propagation is presented, followed with factors influencing small-scale fading in *Section C.3*. In *Section C.4* types of small-scale fading is presented, followed with channel models in S*ections C.5* and *C.6*. Simulation results of the Flat Fading Channel Simulator (FFCS), also see *Chapter 4*, *Section 4.1*, are presented in *Section C.7*, and lastly theoretical BERs for a AWGN channel, slow flat fading Rayleigh fading channel as well as ST coding BERs in a Rayleigh fading channel are presented in *Section C.8*.

C.2 SMALL-SCALE MUTIPATH FADING PROPAGATION

Multipath in the radio channel creates small-scale fading effects. The three most important effects are [1, 7]:

- Rapid changes in signal strength over a small distance or short time interval.
- Random frequency modulation due to varying Doppler shifts on different multipath signals.
- Time dispersion (echoes) caused by multipath propagation delays.

In built-up urban areas, the height of the mobile antennas is well below the height of surrounding structures, so that there exists no single LOS to the BS (*Figure C.1*). Fading occurs due to the movement of the MS, movement of the surrounding objects as well as the multiple paths between the BS and MS (see *Section C.3*). Even when a LOS exists between the MS and BS, multipath still occurs due to reflections from ground and surrounding structures. The incoming radio waves arrive from different directions with different propagation delays. The signal received by the mobile at any point in space may consist of a large number of plane waves having randomly distributed amplitudes, phases, and angles of arrival. These multipath components combine vectorially at the receiver antenna, causing the signal received by the mobile to distort or fade (see *Figure C.2*). Even when a mobile receiver is stationary, the received signal may fade due to movement of surrounding objects in the radio channel. If objects in the radio channel are static, and motion is considered to be only due to that of the mobile, then fading is purely a spatial phenomenon [7].

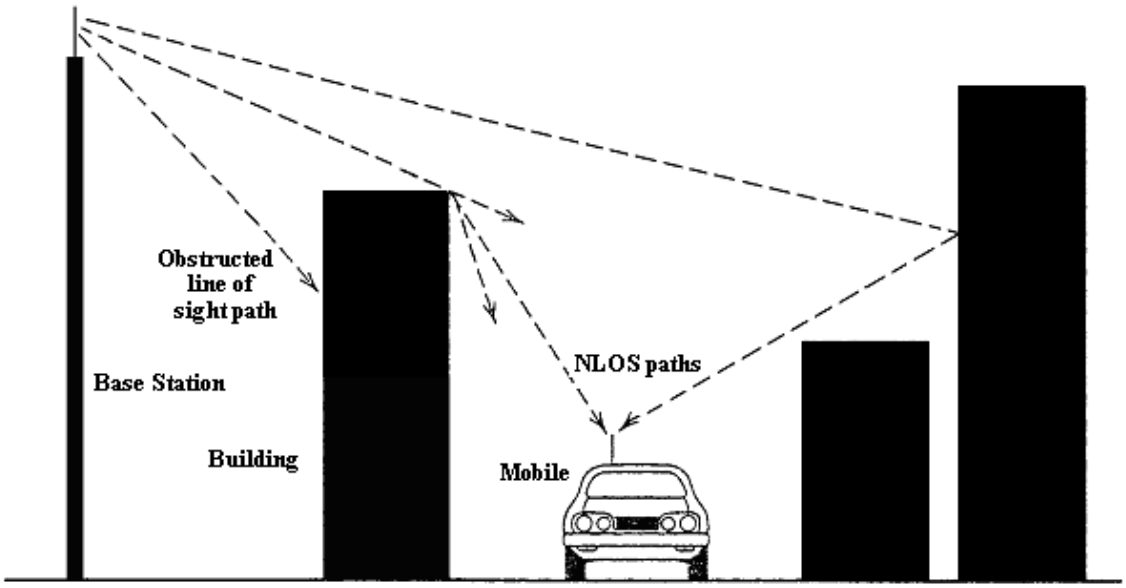

Figure C.1. Illustration of more that one NLOS propagation path towards the mobile unit.

The receiver sees the spatial variations of the resulting signal as temporal variations as it moves through the multipath field. Due to constructive and destructive effects of multipath waves summing at various points in space, a receiver moving at high speed can pass through several fades in a small period of time (See *Figures C.7* and *C.9*). Maintaining good communications can then become very difficult, although passing vehicles or people walking in the vicinity of the mobile can often disturb the field pattern, thereby diminishing the likelihood of the received signal remaining in a deep null for a long period of time. By using multiple antennas at the receiver, the likelihood that both antennas are simultaneously in a fade are less than a single receive antennas scenario, thus resulting in improved reception [9, 73]. Due to the relative motion between the mobile and the BS, each multipath wave experiences an apparent shift in frequency. The shift in received signal frequency due to motion is called the Doppler shift, and is directly proportional to the velocity and direction of motion of the mobile with respect to the direction of arrival of the received multipath wave [1, 6, 7]. See Appendix D for more information on Doppler shift and spread.

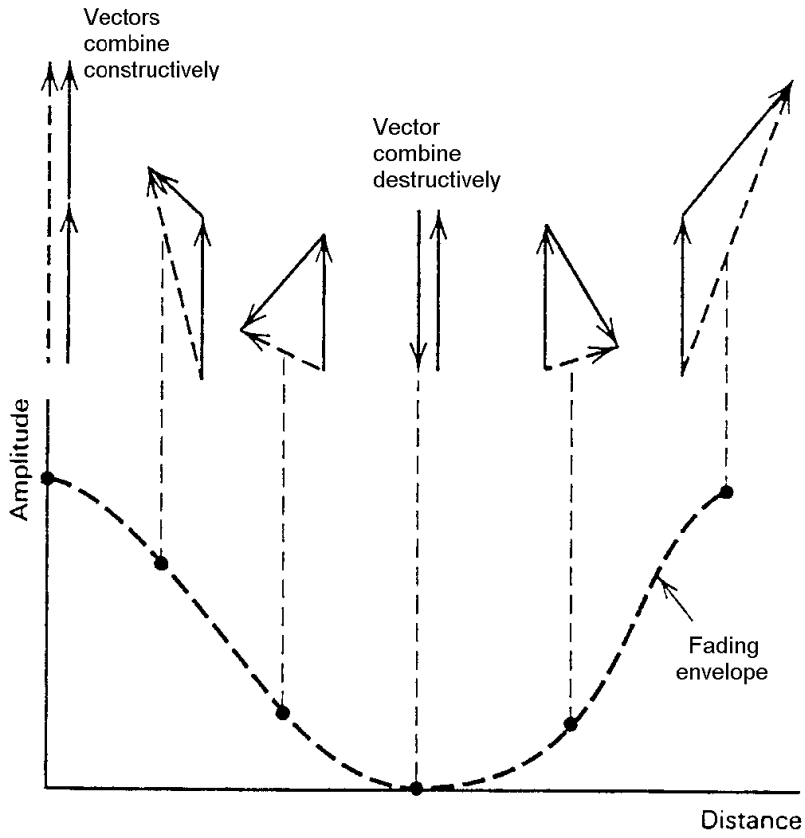

Figure C.2. Envelope fading caused by adding different phases. These phases can be represented by more than two phases adding together, taken from [7].

C.3 FACTORS INFLUENCING SMALL-SCALE MULTIPATH FADING

Many physical factors in the radio propagation channel influence small-scale fading. These include the following:

C.3.1 Multipath propagation

The presence of reflecting objects and scatterers in the channel creates a constantly changing environment that dissipates signal energy in amplitude and phase over time. These effects result in multiple versions of the transmitted signal that arrive at the receiving antenna, displaced with respect to one another in time and spatial orientation. The random phase and amplitudes of the different multipath components cause fluctuations in signal strength, thereby inducing small-scale fading. Multipath propagation often lengthens the time required for the baseband information of the signal to reach the receiver, which can cause signal smearing due to Inter Symbol Interference (ISI). For a more in depth discussion on multipath propagation, see Appendix D.

C.3.2 Speed of the mobile.

The relative motion between the BS and the mobile results in random frequency modulation due to different Doppler shifts on each of the multipath components. Doppler shift will be positive or negative depending on whether the mobile receiver is moving toward or away from the BS. For a more in depth discussion on Doppler shift, see Appendix D.

C.3.3 Speed of surrounding objects.

If objects in the radio channel are in motion, they induce a time varying Doppler shift on multipath components. If the surrounding objects move at a greater rate than the mobile, then this effect dominates the small-scale fading. Otherwise, motion of surrounding objects may be ignored, and only the speed of the mobile need be considered. The *coherence time* defines the "staticness" of the channel, and is directly impacted by the Doppler shift, and Doppler spread. Doppler spread is thus introduced by the time variations in the channel. For a more

in depth discussion on Doppler spread, see Appendix D. Widely used models for the Doppler power spectrum (Doppler spread) of mobile radio channels are the so-called Jakes model [74] and Clarke model [75]. The Doppler spectrum is defined by *Equation (C.1)* and shown in *Figure C.3.*

$$S_C(f) = \begin{cases} \frac{1}{\pi f_d} \frac{1}{\sqrt{1-(f/f_d)^2}} & (|f| \le f_d) \\ 0 & (|f| \le f_d) \end{cases} \qquad \text{(C.1)}$$

where f_d is the maximum Doppler shift. Based on the statistical characteristics of the scattered electromagnetic fields constituting the signal entering the moving receiver, the following geometrical assumptions is made for which Equation C.1 holds:

- The antenna is fixed and employs a vertically polarised omni directional antenna.
- The field incident on the receiver has M_{az} azimuthal plane waves.

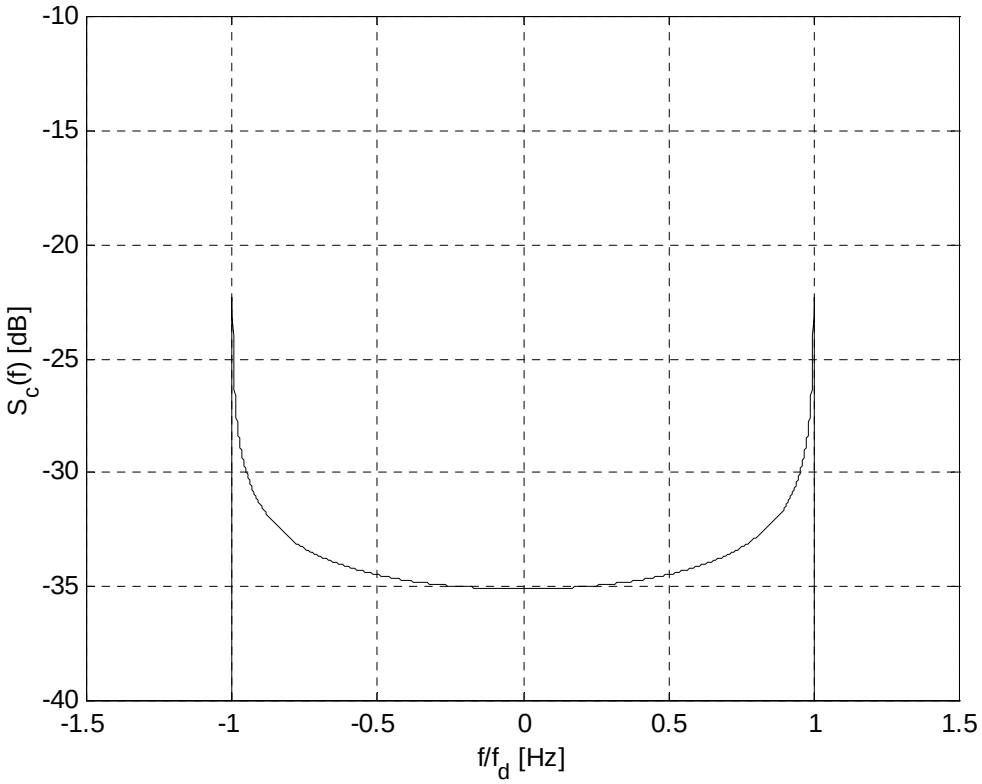

Figure C.3. Doppler power spectrum $S_c(f)$ plot for a baseband mobile radio channel.

- Each of the M_{az} azimuthal plane waves have an arbitrary carrier phase. These phases are assumed to be uniformly distributed between $-\pi$ and π.
- Each of the M_{az} azimuthal plane waves have an arbitrary angle of arrival to the receive antenna.
- The M_{az} azimuthal plane waves have equal average amplitudes, implying an absent LOS path.

C.3.4 The transmission bandwidth of the signal.

If the transmitted radio signal bandwidth is larger than the "bandwidth" of the multipath channel, the received signal will be distorted, but the received signal strength will not fade much over a local area (i.e., the small-scale signal fading will not be significant). As will be shown, the bandwidth of the channel can be quantified by the *coherence bandwidth*, which is related to the specific multipath structure of the channel. The coherence bandwidth is a measure of the maximum frequency difference for which signals are still strongly correlated in amplitude. If the transmitted signal has a narrow bandwidth compared to the channel, the amplitude of the signal will change rapidly, but the signal will not be distorted in time. Thus, the statistics of small-scale signal strength and the likelihood of signal smearing appearing over small-scale distances are very much related to the specific amplitudes and delays of the multipath channel, as well as the bandwidth of the transmitted signal.

C.4 TYPES OF SMALL-SCALE FADING

From the previous sections it is evident that the type of fading experienced by a signal propagating through a mobile radio channel depends on the nature of the transmitted signal with respect to the characteristics of the channel. Depending on the relation between the signal parameters (such as bandwidth, symbol period, etc.) and the channel parameters (such as delay spread and Doppler spread), different transmitted signals will undergo different types of fading.

The time and frequency dispersion mechanisms in a mobile radio channel lead to four possible distinct effects, which are dependant on the nature of the transmitted signal, the channel, and the relative velocity between the BS and the mobile. While multipath delay spread leads to time dispersion and frequency selective fading, Doppler spread leads to frequency dispersion and time selective fading.

C.4.1 Fading effects due to multipath time delay spread

Time dispersion due to multipath causes the transmitted signal to undergo either flat or frequency selective fading.

Flat fading

If the mobile radio channel has a constant gain and linear phase response over a bandwidth, which is greater than the bandwidth of the transmitted signal, then the received signal will undergo flat fading. Thus, the signal bandwidth is small in comparison to the coherence bandwidth. In flat fading, the multipath structure of the channel is such that the spectral characteristics of the transmitted signal are preserved at the receiver. However, the strength of the received signal changes with time, due to fluctuations in the gain of the channel caused by multipath. This is observed as a received signal with varying gain over time, with the spectrum of the transmission practically preserved. Typical flat fading channels cause deep fades, and thus may require 20 or 30 dB more transmitter power to achieve low bit error rates during times of deep fades, as compared to systems operating over non-fading channels. To summarize, a signal undergoes flat fading if

$$BW_s << BW_c \quad \text{and}$$

$$T_s >> \vartheta_\tau \qquad \text{(C.2)}$$

where T_s is symbol period, BW_s the bandwidth of the transmitted modulation, ϑ_τ the channel RMS delay spread (see Appendix D) and BW_c the channel coherence bandwidth.

Frequency Selective Fading

If the channel possesses a constant-gain and linear phase response over a bandwidth that is smaller than the bandwidth of transmitted signal, then the channel creates frequency selective fading on the received signal. Thus, the signal bandwidth is large in comparison to the coherence bandwidth. Under such conditions, the channel impulse response has a multipath delay spread which is greater than the reciprocal bandwidth of the transmitted message waveform. When this occurs, the received signal includes multiple versions of the transmitted waveform, which are attenuated (faded) and delayed in time, and hence the received signal is distorted. Viewed in the frequency domain, certain frequency components in the received signal spectrum have greater gains than others. Frequency selective fading channels are much more difficult to model than flat fading channels since each multipath signal must be modelled and the channel must be considered to be a linear filter. It is for this reason that wideband multipath measurements are made and models are developed from these measurements.

To summarize, a signal undergoes frequency selective fading if

$$BW_s > BW_c \quad \text{and}$$

$$T_s < \vartheta_\tau \qquad \text{(C.3)}$$

A common rule of thumb is that a channel is flat fading if $T_s \geq 10\ \vartheta_\tau$ [1] and a channel is frequency selective if $T_s < 10\ \vartheta_\tau$ [1].

C.4.2 Fading effects due to Doppler spread

Depending on how rapidly the transmitted baseband signal changes compared to the channel's rate of change, a channel may be classified either as a fast fading or slow fading channel.

Fast Fading

In a fast fading channel, the channel impulse response changes rapidly within the symbol duration. That is, the coherence time of the channel is smaller than the symbol period of the transmitted signal. This causes frequency dispersion (also called time selective fading) due to Doppler spreading, which leads to signal distortion. Viewed in the frequency domain, signal distortion due to fast fading increases with increasing Doppler spread relative to the bandwidth of the transmitted signal. Therefore, a signal undergoes fast fading if

$$T_s > T_c \quad \text{and}$$

$$BW_s < BW_d \tag{C.4}$$

Where BW_d is the Doppler spread bandwidth. It should be noted that when a channel is specified as a fast or slow fading channel, it does not specify whether the channel is flat fading or frequency selective in nature. Fast fading only deals with the rate of change of the channel due to motion. In the case of the flat fading channel, we can approximate the impulse response to be simply a delta distribution (no time delay). Hence, a flat, fast fading channel is a channel in which the amplitude of the delta functional varies faster than the rate of change of the transmitted baseband signal. In the case of a frequency selective, fast fading channel, the amplitudes, phases, and time delays of anyone of the multipath components vary faster than the rate of change of the transmitted signal. In practice, fast fading only occurs for very low data rates.

Slow Fading

In a slow fading channel, the channel impulse response changes at a rate much slower than the transmitted baseband signal. In this case, the channel may be assumed to be static over one or several reciprocal bandwidth intervals. In the frequency domain, this implies that the Doppler spread of the channel is much less than the bandwidth of the baseband signal. Therefore, a signal undergoes slow fading if

$$T_s << T_c \quad \text{and}$$

$$BW_s >> BW_d \tag{C.5}$$

It should be stated here that the velocity of the mobile (or velocity of objects in the channel) and the baseband signalling determines whether a signal undergoes fast fading or slow fading. It should also be emphasized that fast and slow fading deal with the relationship between the time rate of change in the channel and the transmitted signal, and not with propagation path loss models.

C.5. AWGN CHANNEL MODELS

C.5.1. Probability density function and spectral characteristics

An unavoidable limiting factor in the performance and capabilities of communication systems is AWGN. Understanding the nature of noise is therefore crucial if effective counter measures, such as channel coding, are to be designed.

Degradation of communication systems' performance in noisy channel conditions can be attributed to as variety of noise sources, e.g. interference from other communication systems, thermal noise and amplifier noise. The primary statistical characteristics of the resultant noise caused by adding the above mentioned noise sources, is that its amplitude exhibits a Gaussian distribution with a Probability Density Function (PDF) given by

$$pdf(z) = \frac{1}{\sigma_n \sqrt{2\pi}} \exp\left(-\frac{z^2}{2\sigma_n^2}\right) \tag{C.6}$$

where z is the noise amplitude, and σ_z^2 the noise variance power. The principle spectral characteristics of AWGN are that it has an essentially flat two-sided PSD for frequencies up to approximately 10^{12} Hz.

C.5.2. Obtaining Gaussian samples with required noise variance

When investigating the performance of communication systems in typical mobile communication channel conditions, two quantities, namely the SNR and the E_b/N_0 value (measured in dB), are of importance. Used more commonly in everyday speech, the SNR defines the ratio of average transmitted signal power to noise power at the receiver output. However, it is meaningless unless the noise bandwidth of the receiver is specified. Consequently the SNR is frequently normalised with respect to the noise bandwidth, resulting in the quantity E_b/N_0, which then becomes the dependent variable in the performance measurements. By stipulating the E_b/N_0 value for a specific performance measurement set up, it is possible to calculate the variance σ_n^2 of the Gaussian noise samples required to realise the correct AWGN channel conditions. Given the transmitted signal's bandwidth BW_s, the following relationship between the SNR and E_b/N_0 of uncoded binary communication systems holds:

$$SNR = \frac{\sigma_s^2}{\sigma_n^2} \quad (In\ the\ bandwidth\ BW_s) = \frac{E_b \cdot R_b}{N_0 \cdot BW_s} \tag{C.7}$$

where σ_s^2 is the variance (power) of the transmitted signal, σ_n^2 is the variance (power) of the required Gaussian noise samples, E_b is the energy in an uncoded bit, R_b is the uncoded bit rate and N_0 is the single sided PSD level of the AWGN.

Manipulation of *Equation (C.7)* can be shown to give [4]

$$psf_n = \frac{\sigma_s^2 \cdot f_{samp}}{10^{\left(\frac{1}{10}\cdot\frac{E_b}{N_0}\right)} \cdot 2R_b} \tag{C.8}$$

where f_{samp} is the sampling rate of the transmitter. Thus, the Gaussian distributed samples are scaled with a power scaling factor psf_n to produce Gaussian noise samples with variance of σ_n^2, which in turn produces the required E_b/N_0 level.

C.5.3. Probability of error for AWGN channels

The probability of a bit error of many modulation schemes in an AWGN channel is found by using the Q-function [6]. For a BPSK signal constellation the probability of a bit error is given as [1]

$$P_{e,BPSK}^{AWGN} = Q\left(\sqrt{2\Gamma}\right) \qquad \text{(C.9)}$$

where $\Gamma = E_b / N_0$ is the SNR per bit.

C.6. FLAT FADING CHANNEL MODELS

Radio channels can be modelled as a wide variety of distributions, such as an AWGN channel, a Rayleigh channel, a Rician channel, a log-normal channel etc. Due to the NLOS and LOS components, mobile radio channels are often modelled as a Rayleigh or Rician channel. Thus, only these two distributions are considered in this dissertation.

C.6.1. Rayleigh fading distribution

In mobile radio channels, the Rayleigh distribution is commonly used to describe the statistical time varying nature of the received envelope of a flat fading signal, or the envelope of an individual multipath component. It is well known that the envelope of the sum of two quadrature Gaussian noise signals obeys a Rayleigh distribution. *Figure C.4* shows a Rayleigh distributed signal envelope as a function of time. The Rayleigh distribution has a PDF given by

$$pdf(z) = \begin{cases} \dfrac{z}{\sigma_z^{\,2}} \exp\left(-\dfrac{z^2}{2\sigma_z^{\,2}}\right) & for \quad 0 \le z \le \infty \\ 0 & for \quad z < 0 \end{cases} \qquad \text{(C.10)}$$

where σ_z is the Root Mean Square (RMS) value of the received signal amplitude z before envelope detection, and σ_Z^2 is the power of the received signal before envelope detection.

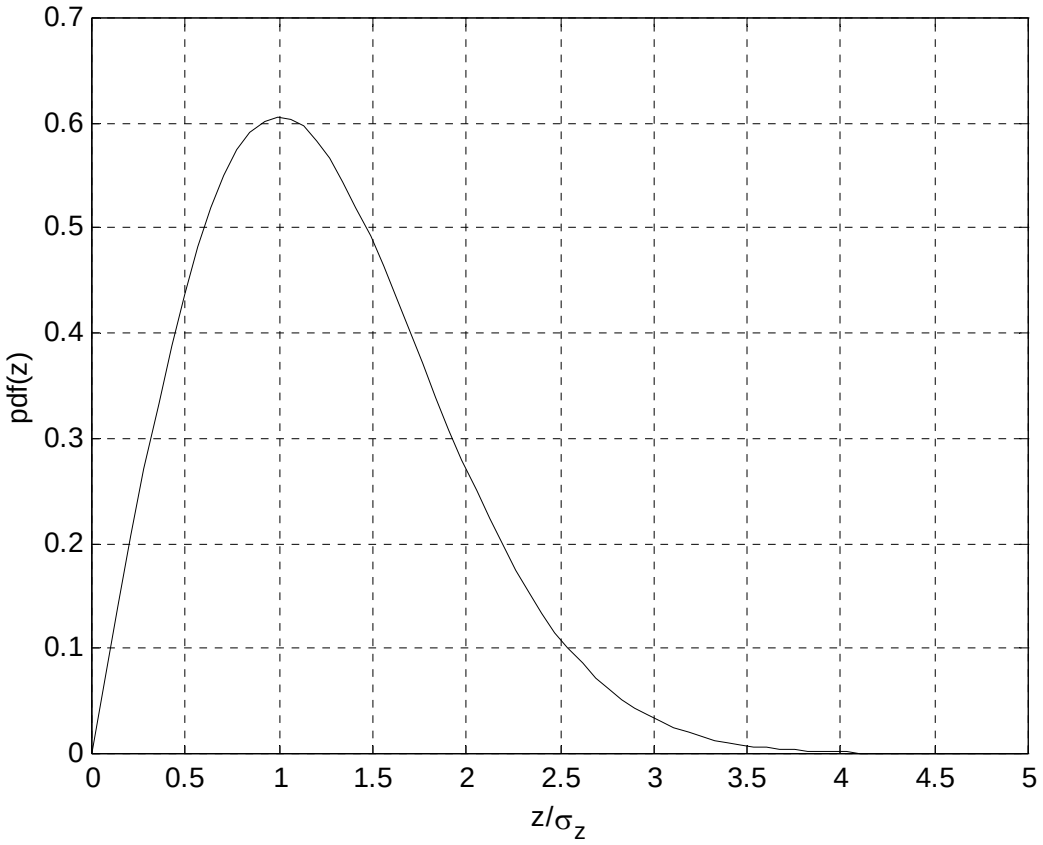

Figure C.4. PDF of a Rayleigh distribution.

C.6.2. Rayleigh fading probability of error

The probability of a bit error of coherent BPSK in a slow Rayleigh fading channel is given as [1]

$$P_{e,BPSK}^{RAY} = \frac{1}{2}\left[1-\sqrt{\frac{\Gamma}{1+\Gamma}}\right] \qquad \text{(C.11)}$$

where $\Gamma = E_b/N_0$ is the SNR per bit. The theoretical probability of error graphs for *Equations (C.9)* and *(C.11)* are presented in *Section C.8, Figure C.19* in order to show the performance difference between modulation techniques' performance in Rayleigh and AWGN channels.

C.6.3. Rician fading distribution

When there is a dominant stationary (non-fading) signal component present, i.e. a LOS propagation path, the small-scale fading envelope distribution can be modelled as Rician. In such a situation, random multipath components arriving at different angles are superimposed on a stationary dominant signal. At the output of an envelope detector, this has the effect of adding a Direct Current (DC) component to the envelope.

Just as for the case of detection of a sine wave in thermal noise, the effect of a dominant signal arriving with many weaker multipath signals gives rise to the Rician distribution. As the dominant signal becomes weaker, the composite signal resembles a noise signal with a Rayleigh fading envelope. Thus, the Rician distribution changes to a Rayleigh distribution when the LOS component fades away. The Rician distribution is given by

$$pdf(z) = \begin{cases} \dfrac{z}{\sigma_z^2}\exp\left(-\dfrac{(z^2+2K}{2\sigma_z^2}\right) I_0\left(\dfrac{\sqrt{2K}\ z}{\sigma_z^2}\right) & for \quad 0 \le z \le \infty \\ 0 & for \quad z < 0 \end{cases} \qquad \text{(C.12)}$$

The parameter $\sqrt{2K}$ denotes the peak amplitude of the dominant signal and $I_0(\bullet)$ is the modified zero-order Bessel function of the first kind. The Rician factor *K* denotes the ratio between the direct LOS signal component and the scatter component of the signal (see *Chapter 4, Section 4.1.1.*).

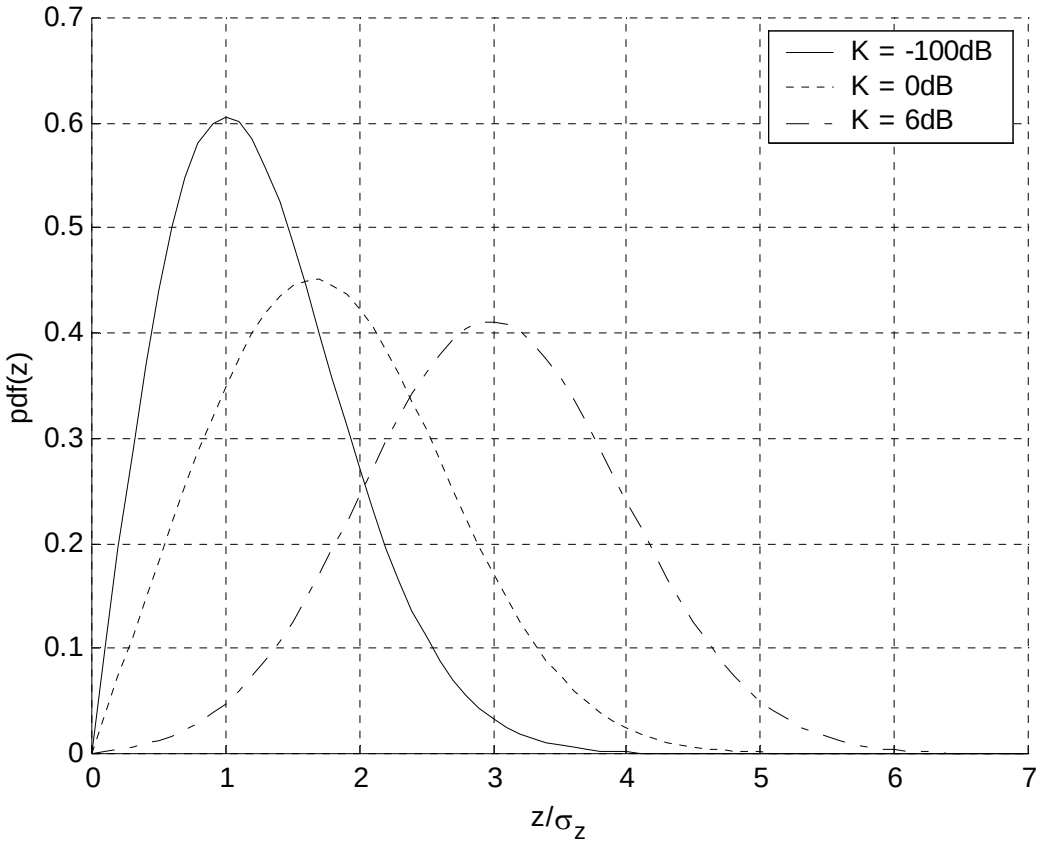

Figure C.5. Rician distribution for a LOS component (K) of -100 dB, 0 dB and 6 dB.

C.7. SIMULATION RESULTS OF THE FADING CHANNEL SIMULATOR

Simulation results for the FFCS presented in *Chapter 4*, *Section 4.1*, are presented in this section. As input to the FFCS shown in *Chapter 4*, *Section 4.1*, *Figure 4.1*, an unmodulated 1000Hz signal was used, sampled at 1MHz. It should also be stated that the received signal had constant and linear phase over the symbol duration. The following simulations were obtained for different values of the Rician constant (*K*) and speed of the mobile (different Doppler frequencies).

C.7.1. The received signal envelope

From *Figures C.6* to *C.9*, it can be seen that the received signal's envelope is fading if the channel is purely Rayleigh distributed (K = -100dB) and is much more constant with a Rician distribution (K = 6dB) as a result of the direct *LOS* component present in the Rician distribution. For a more in depth discussion on channel fade durations and fading statistics, see [1]. Comparing *Figures C.6* and *C.7*, it is evident that a low mobile speed has less fades and longer fade durations in comparison to a fast moving mobile that has significant more fades and much shorter fade durations.

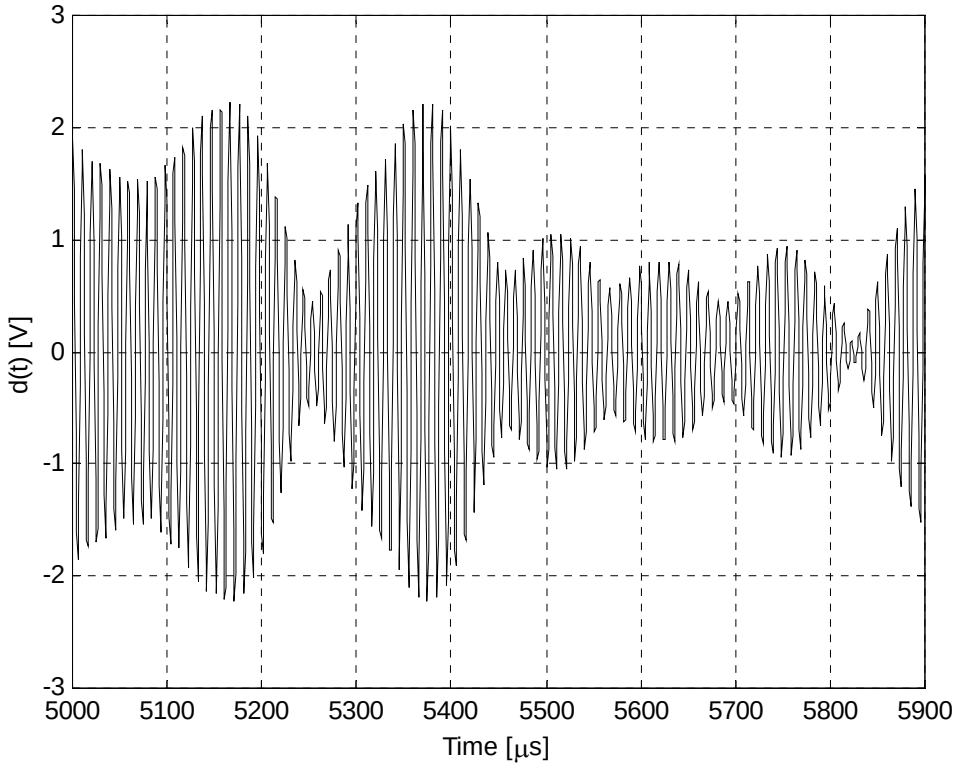

Figure C.6. Plot of a fading signal with K = -100dB and f_d = 33Hz.

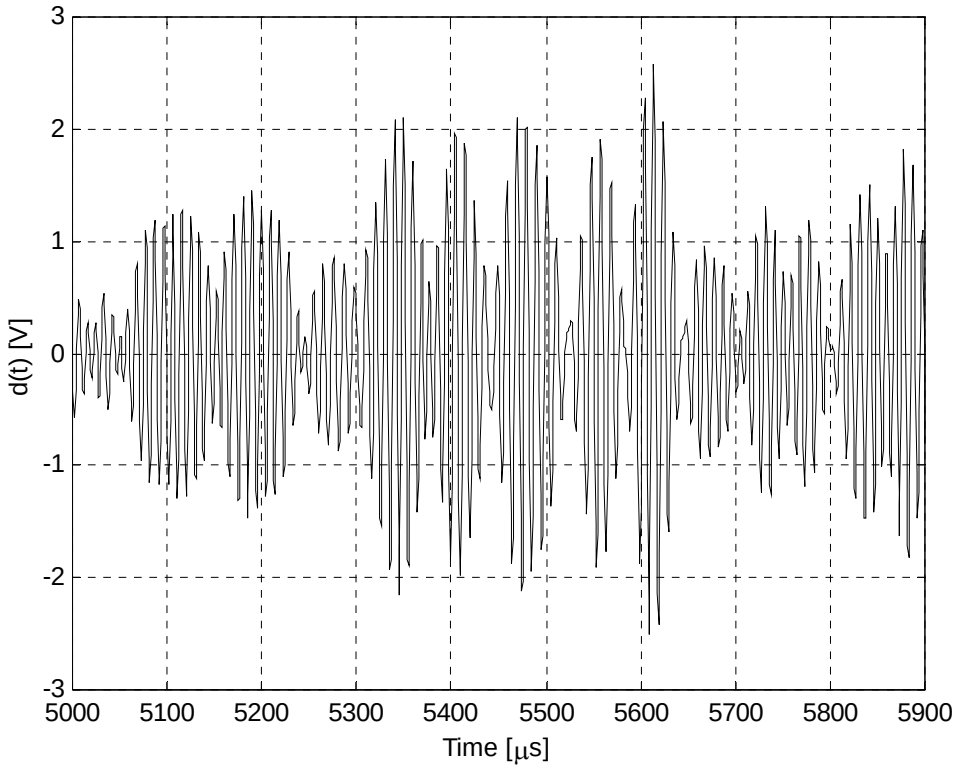

Figure C.7. Plot of a fading signal with K = -100dB and f_d = 100Hz.

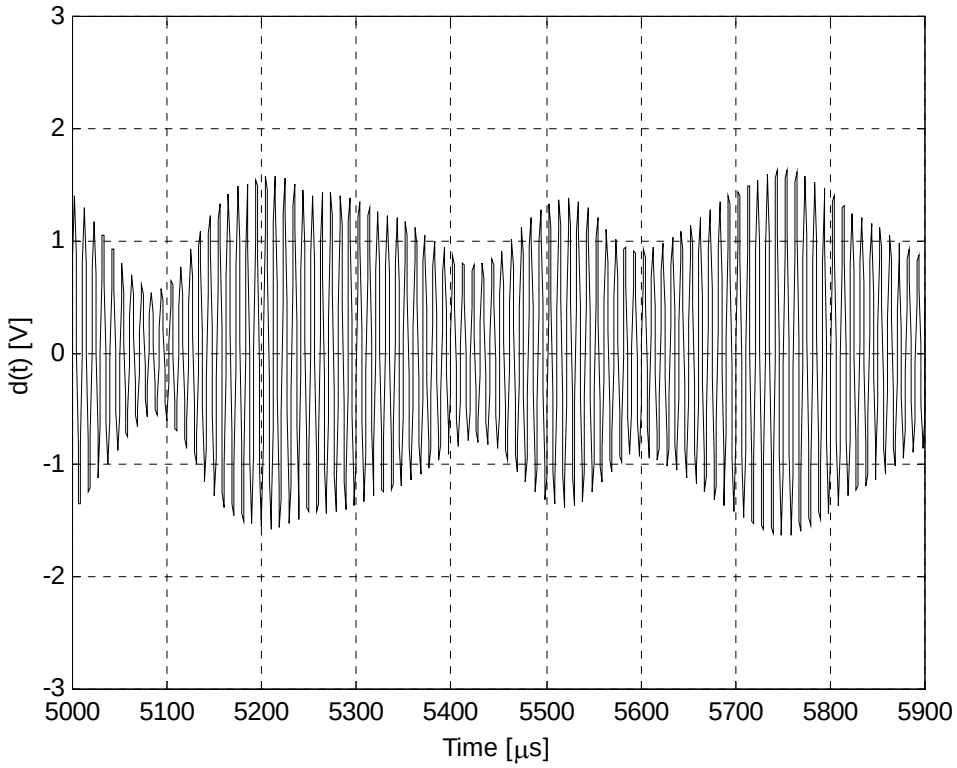

Figure C.8. Plot of a fading signal with K = 6dB and f_d = 33Hz.

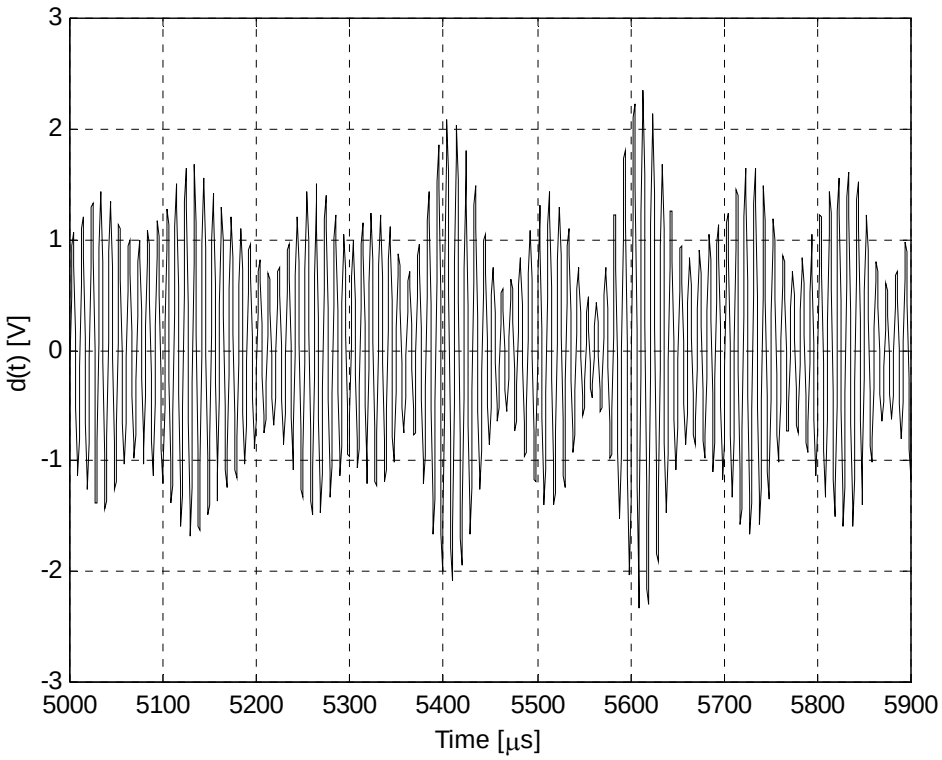

Figure C.9. Plot of a fading signal with K = 6dB and f_d = 100Hz.

C.7.2. The power spectrum of the received signal

From *Figures C.10* and *C.11* it is evident that the single frequency component in an unmodulated carrier is broadened to the Doppler power spectrum (compare with *Figure C.3* in *Section C.3*).

This Doppler spread is a function of the speed of the mobile (see Appendix D). The higher the speed of the mobile, the more frequency spread is introduced to the fading signal and visa versa. From *Figures C.12* and *C.13*, the presence of a direct *LOS* component (K) is seen as a single carrier component in the frequency spectrum at f = 1000Hz. As K becomes progressively larger, the peak power of the Doppler sidebands (i.e. frequency spread) is reduced compared to the peak power of the single carrier component. Thus, when K becomes sufficiently large, most power in the frequency spectrum lies within the single frequency component due to the input signal's frequency, showing that high *LOS* components counter the effects of Doppler spreading.

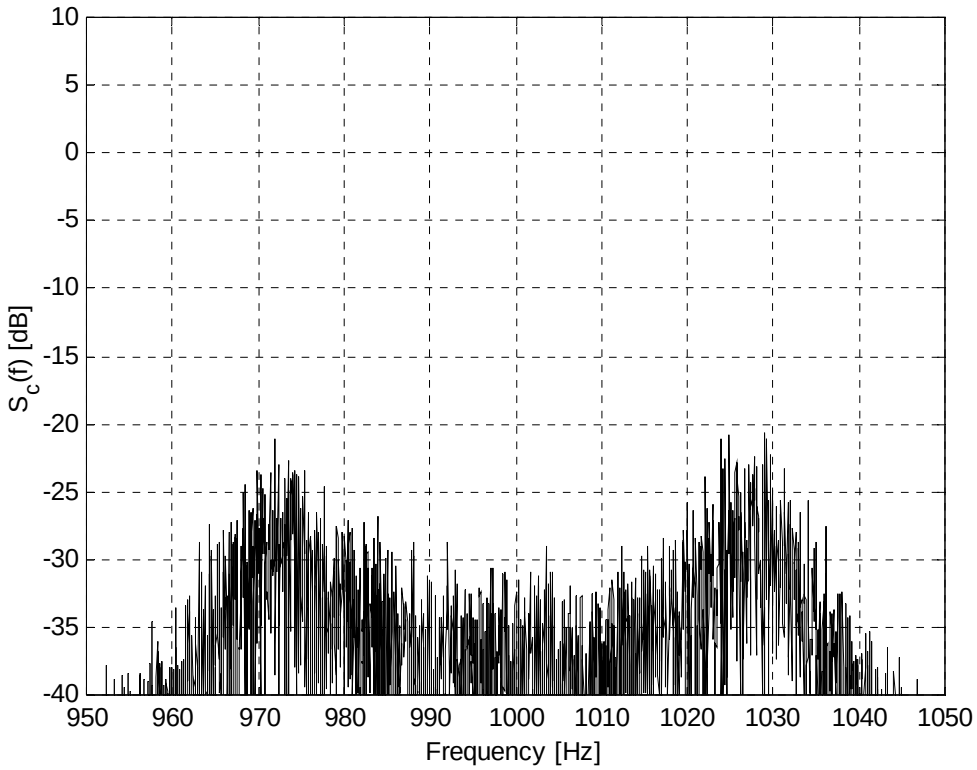

Figure C.10. The power spectrum of the fading signal shown in Figure C.6, with K = -100dB and f_d = 33Hz.

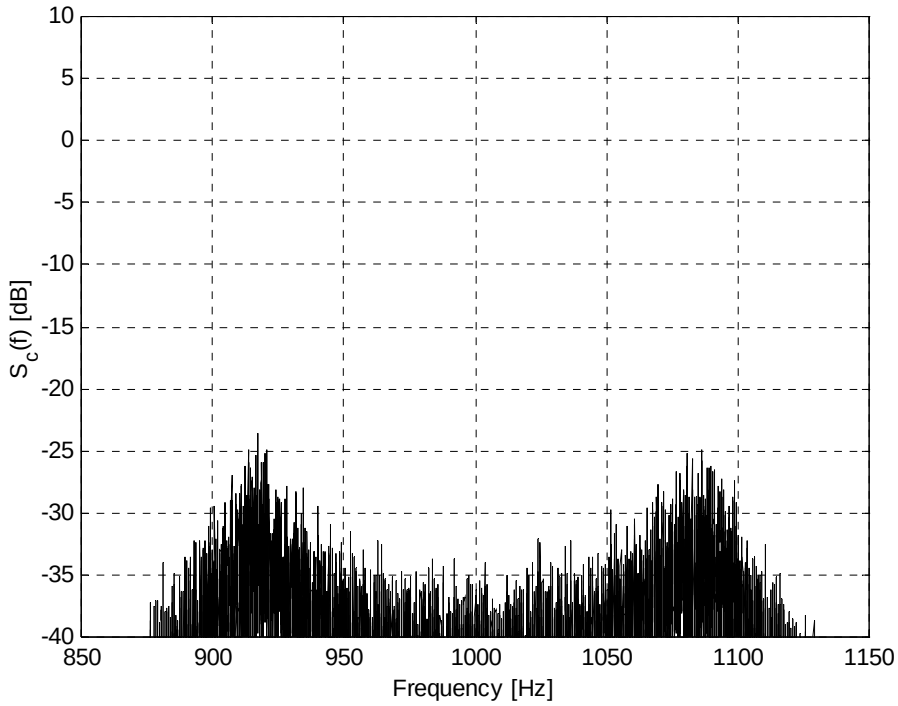

Figure C.11. The power spectrum of the fading signal shown in Figure C.7, with K = -100dB and f_d = 100Hz.

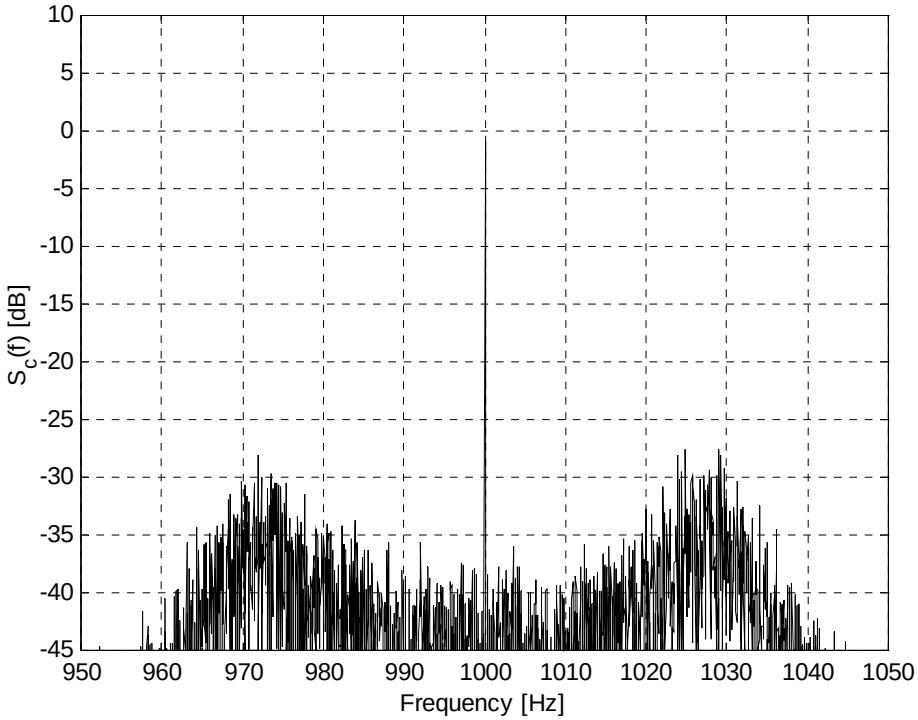

Figure C.12. The power spectrum of the fading signal shown in Figure C.8, with K = 6dB and f_d = 33Hz.

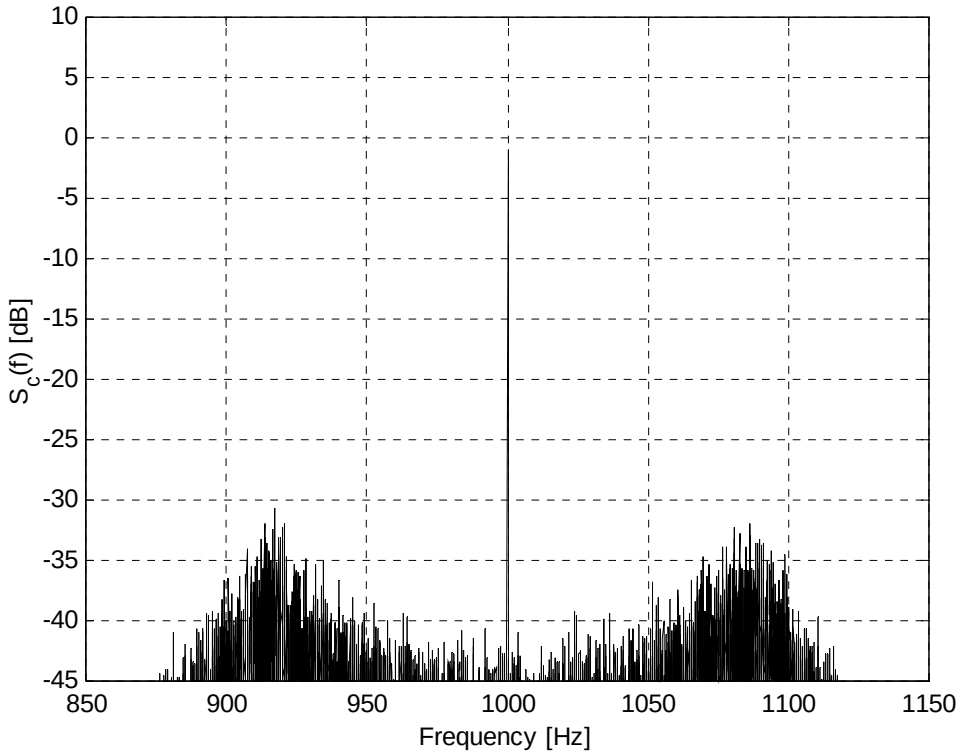

Figure C.13. The power spectrum of the fading signal shown in Figure C.9, with K = 6dB and f_d = 100Hz.

C.7.3. The PDF of the received signal

From *Figures C.14* to *C.17* it can be seen that the received signal's envelope is Rayleigh distributed when K = -100dB, and Rician distributed when K becomes larger (compare with *Figures C.4* and *C.5* in *Section C.6*). Eventually, when K = 6dB, the Rician distribution tends to be a Gauss distribution with a mean of 3 and variance of approximately 1. This is merely a result of the direct *LOS* component present in the Rician distribution. Because of identical distributions in *Figures C.14* and *C.15*, as well as *Figures C.16* and *C.17*, it can be stated that the received signal envelope is practically independent of the mobile speed (Doppler spread) in the presence of a dominant LOS signal component.

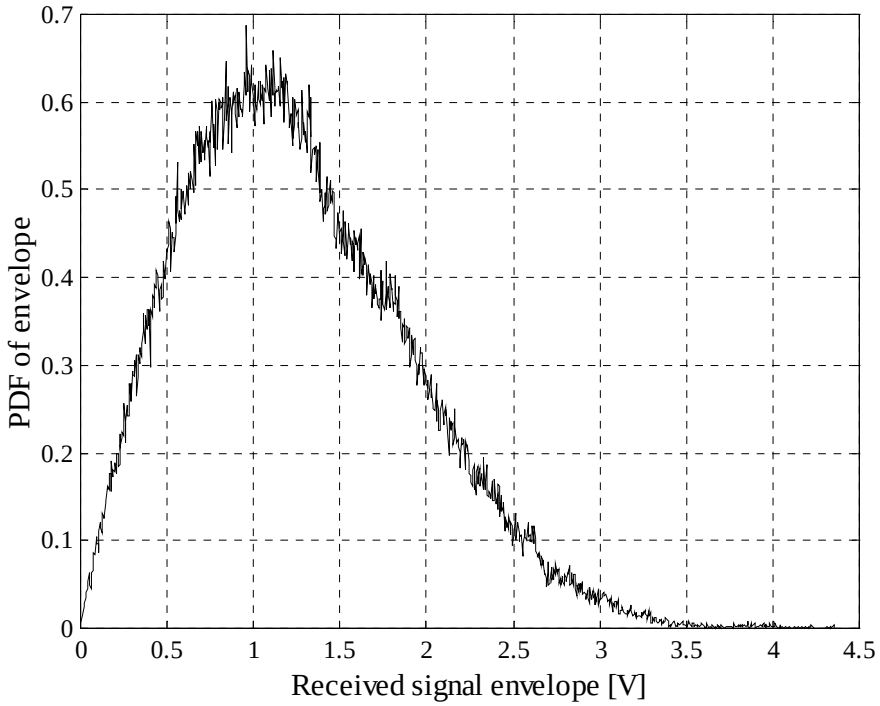

Figure C.14. The PDF of the fading signal's envelope in Figure C.6, with K = -100dB and f_d = 33Hz.

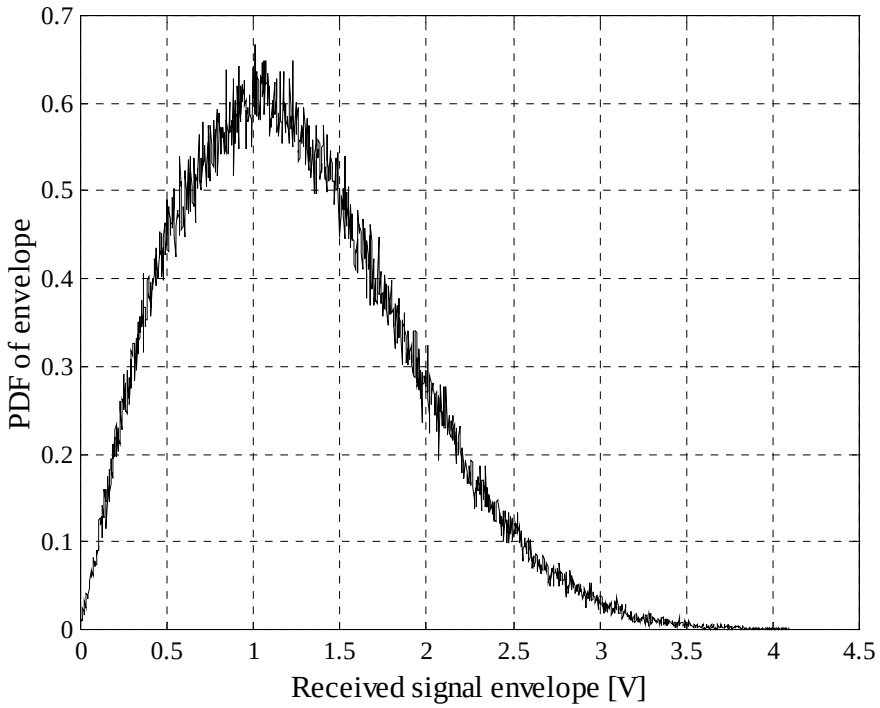

Figure C.15. The PDF of the fading signal's envelope in Figure C.7, with K = -100dB and f_d = 100Hz.

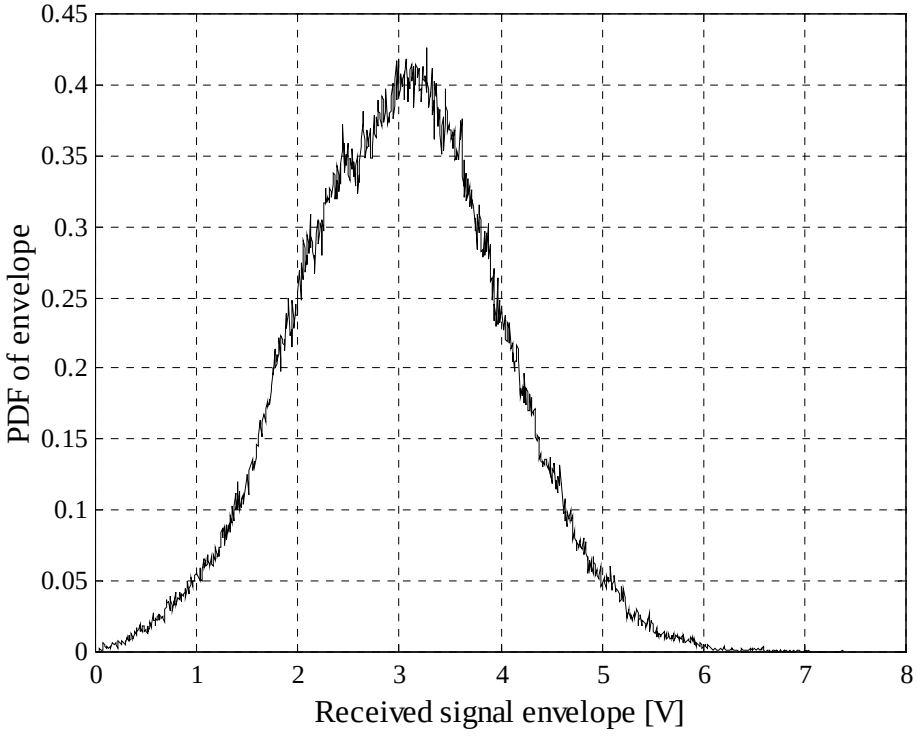

Figure C.16. The PDF of the fading signal's envelope in Figure C.8, with K = 6dB and f_d = 33Hz.

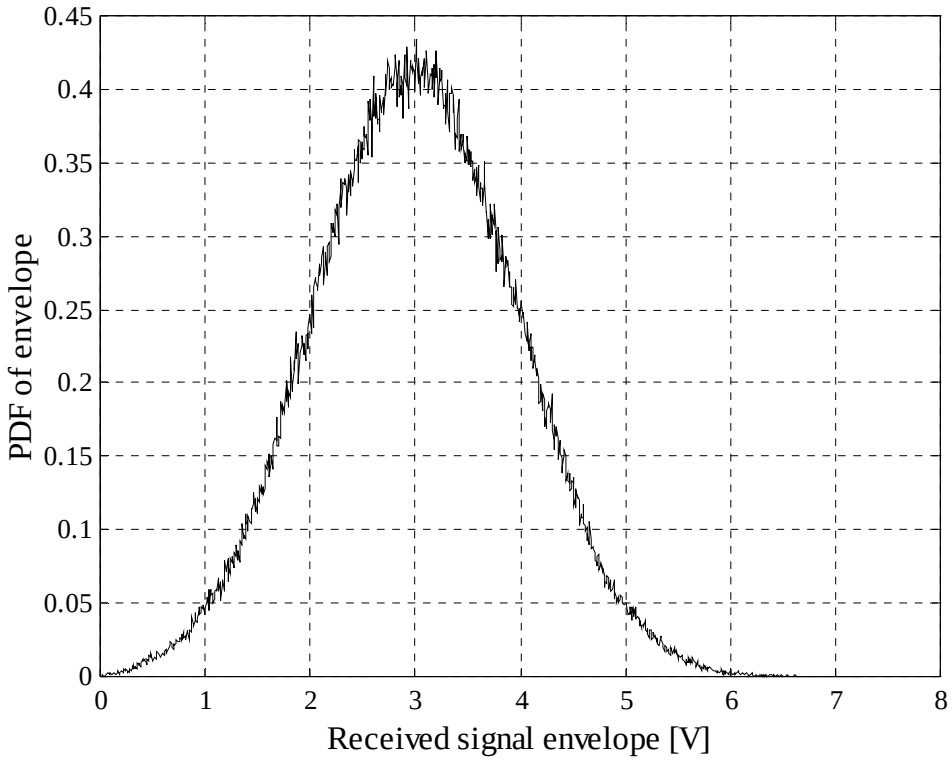

Figure C.17. The PDF of the fading signal's envelope in Figure C.9, with K = 6dB and f_d = 100Hz.

C.8. THEORETICAL BERs

In *Chapter 2*, *Equations (2.24)* and *(2.25)* were presented for ST coding error probabilities of BPSK and QPSK in a Rayleigh fading channel, respectively. These equations are plotted in *Figure C.18* for comparison purposes. The probability of error for a flat fading Rayleigh channel (see *Section C.6.2, Equation (C.11)*), is also included as a reference graph. Also note that a 3dB difference exists between the BPSK and QPSK modulation techniques. The probability of a bit error of coherent BPSK in a Rayleigh fading channel was given in *Section C.6.2, Equation (C.11),* whereas the probability of a bit error for a BPSK signal constellation in an AWGN channel is given by *Equation (C.9).* The theoretical probability of error graphs for *Equations (C.9)* and *(C.11)* are presented in *Figure C.19* and will henceforth serve as upper and lower bounds in the subsequent performance analysis of the proposed DSSTS schemes.

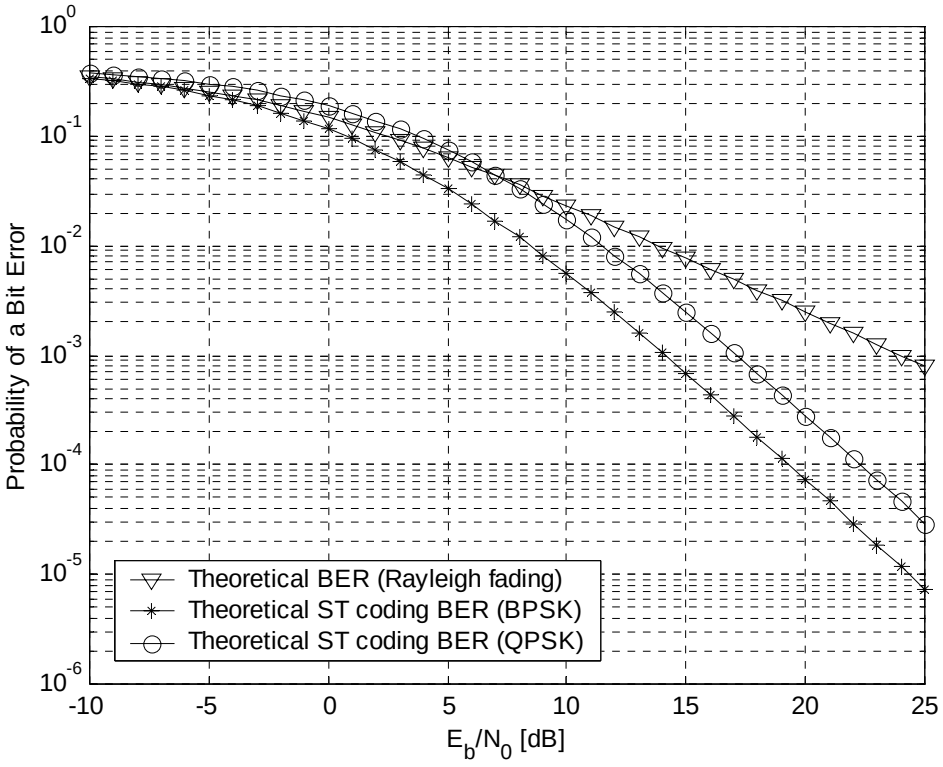

Figure C.18. Comparison of the simulation of a uncoded system, BPSK ST – and QPSK ST code's probability of error in a Rayleigh fading channel [24].

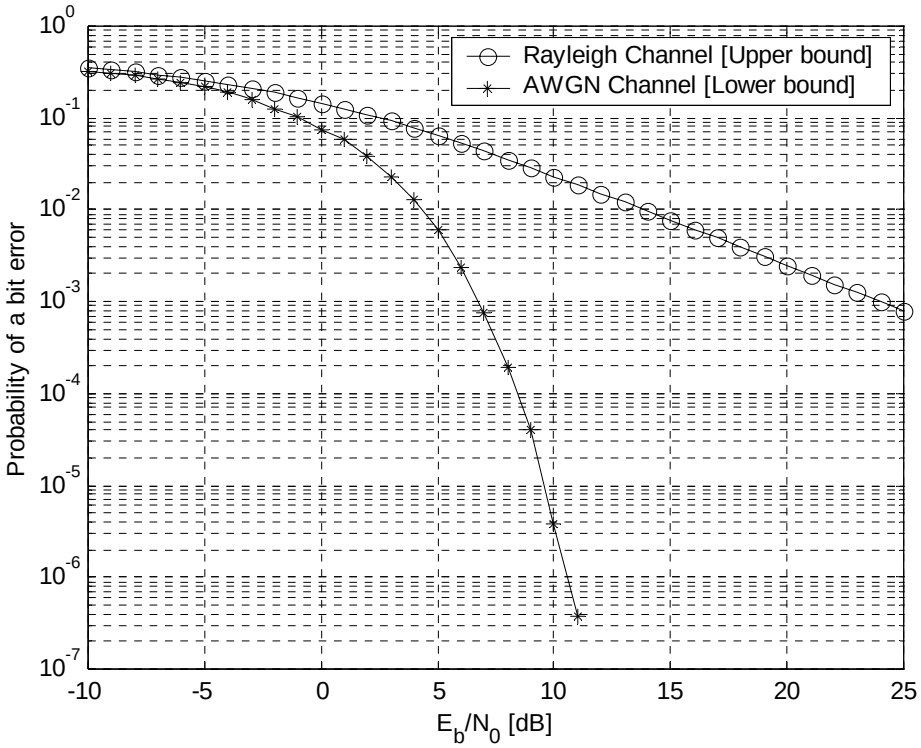

Figure C.19. Benchmark probability of error results for a BPSK system in Rayleigh as well as AWGN channel conditions.

APPENDIX D

CHANNEL EFFECTS, MATHEMATICAL ANALYSIS

D.1 APPENDIX OVERVIEW

In Appendix D an overview of different channel effects are discussed. In *Section D.2*, the Doppler effect is explained, while a statistical formulation of channel effects that occur due to multipath fading, is presented in *Section D.3* and *Section D.4*. In *Sections D.5* and *D.6* the concepts of delay spread and Doppler spread are introduced, respectively. Lastly, Clarke's fading model simulator is presented in *Section D.8* as well as the derivation of the scaling factors that were used in Chapter 4.

D.2 DOPPLER SHIFT

Signal fading is essentially a spatial phenomenon that manifests itself in the time domain as fluctuations occur in receive power as relative movement occur between the transmitter and receiver. With reference to *Figure D.1*, assume that a mobile is moving at a constant velocity v between points X and Y, receiving signals from a distant stationary source S. Assuming that X and Y are far apart, the receive angles at both point X and Y

are approximately θ. If d is the path length from X to Y, the difference in path lengths travelled by the waves from the source S to the mobile at points X and Y is $\Delta l = d\cos\theta = v\Delta t\cos\theta$ where Δt is the time required for the mobile to travel from point X to Y. Thus, the phase change in the received signal due to the difference in path length is given in *Equation (D.1)*

$$\Delta\Phi = \frac{2\pi\Delta l}{\lambda} = \frac{2\pi v\Delta t}{\lambda}\cos\theta \qquad \text{(D.1)}$$

The change in frequency, or Doppler shift f_d , due to the motion of the mobile, is given by *Equation (D.2)*

$$f_d = \frac{1}{2\pi}\frac{\Delta\Phi}{\Delta t} = \frac{v}{\lambda}\cos\theta \qquad \text{(D.2)}$$

From *Equation (D.2)* it can be seen that the Doppler shift is dependant on the speed and direction of the moving mobile. If the mobile moves towards the source S, the Doppler frequency is positive (i.e. the apparent received frequency increases), and negative as it moves away from the source (i.e. the apparent received frequency decreases).

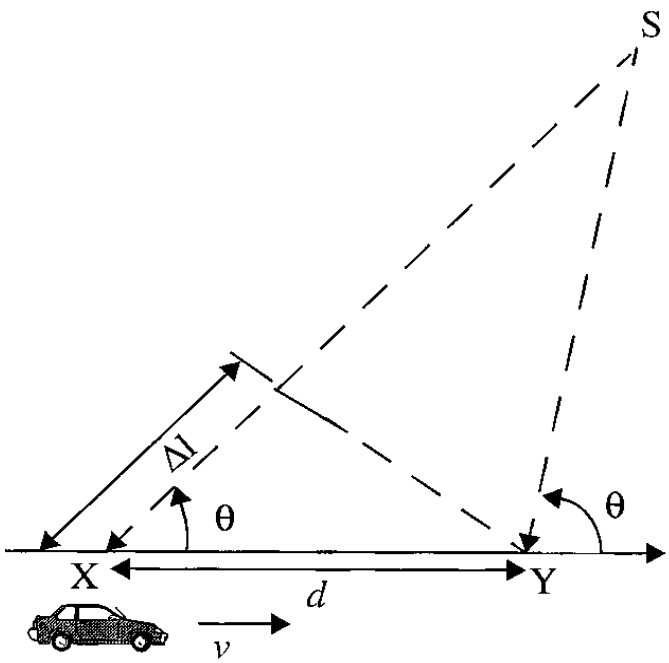

Figure D.1. Illustration of the Doppler effect, taken from Rappaport, pp.180 [1].

D.3 IMPULSE RESPONSE MODEL OF A MULTIPATH CHANNEL

If an extremely short pulse, ideally an impulse, is transmitted over a time-varying multipath channel, the received signal might appear as a train of pulses (*Figure D.2*). Note that [6] is the source for *Sections D.3* and *D.4*. Hence, two characteristics of a time-varying multipath channel that can be seen in *Figure D.2* are:

- Time spread of the signal is introduced.
- The nature of the all the multipaths varies with time in accordance to the environmental changes.

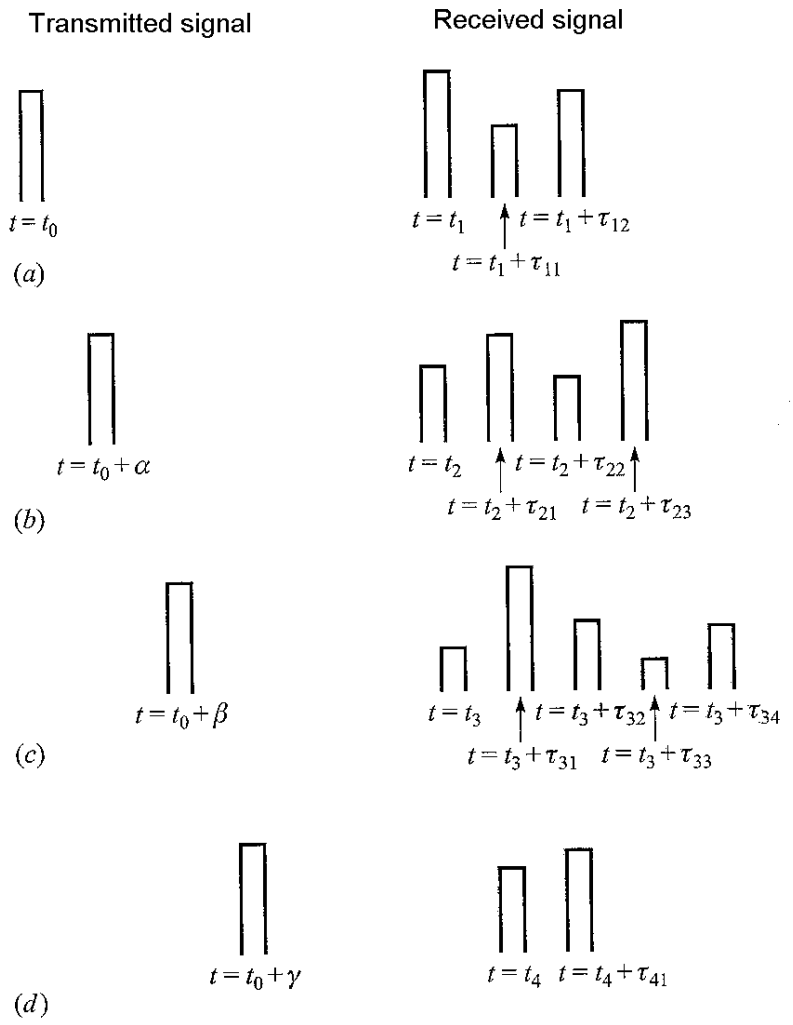

Figure D.2. Example of the response of a time variant multipath channel. Note that the same pulse in (a) to (d) is received differently in each case because of multipath, taken from Proakis, pp. 801 [6].

The time variations in the channel, as seen in *Figure D.2*, appear to be unpredictable to the user of the channel. For this reason, a time variant multipath channel is characterised statistically.

Assume a transmitted signal to be of the form

$$u(t) = \mathrm{Re}[\, u_l(t) \exp(\; j2\pi f_c t)] \tag{D.3}$$

A received band pass signal, having L multipaths that faded and introduced time spread in the signal can be represented by

$$x(t) = \sum_i^L \beta_i(t) u[t - \tau_i(t)] \tag{D.4}$$

where $\beta_i(t)$ represents the attenuation of the i^{th} path with a time delay of $\tau_i(t)$. Substitution of *Equation (D.3)* into *Equation (D.4)* yields

$$x(t) = \mathrm{Re}\left(\left\{ \sum_i^L \beta_i(t) e^{-j2\pi f_c \tau_i(t)} u_l[t - \tau_i(t)] \right\} e^{j2\pi f_c t} \right) \tag{D.5}$$

From *Equation (D.5)*, it is apparent that the equivalent low-pass received signal is

$$d_l(t) = \sum_i^L \beta_i(t) e^{-j2 f_c \tau_i(t)} u_l[t - \tau_i(t)] \tag{D.6}$$

But, $d_l(t)$ is a response of an equivalent low-pass channel to an equivalent low-pass signal $u_l(t)$. Thus, the equivalent low-pass channel is described by the time-variant impulse response in discrete form in *Equation (D.7)*

$$c(\tau; t) = \sum_i^L \beta_i(t) e^{-j2 f_c \tau_i(t)} \delta[t - \tau_i(t)] \tag{D.7}$$

In integral form, the received signal $d(t)$ is represented by

$$d(t) = \int_{-\infty}^{\infty} \beta(\tau;t)u(t-\tau)d\tau \tag{D.8}$$

where $\beta(t;\tau)$ denotes the attenuation of the signal with a delay time of τ at time instant t. By substitution of *Equation (D.3)* into *Equation (D.8)*, the received signal in integral form is

$$d(t) = \mathrm{Re}\left(\left\{ \int_{-\infty}^{\infty} \beta(\tau;t) e^{-j2\pi f_c \tau} u_l(t-\tau) d\tau \right\} e^{j2\pi f_c t} \right) \tag{D.9}$$

Because *Equation (D.9)* represents the convolution of $u_l(t)$ with an equivalent low-pass time variant impulse response, it follows that

$$c(\tau;t) = \beta(\tau;t)e^{-j2\pi f_c \tau} \tag{D.10}$$

where $c(\tau;t)$ represents the response of the channel at time t due to an impulse applied at time instant $(t - \tau)$. For example, assume an unmodulated carrier at frequency f_c. Then $u_l(t) = 1$ for all t and the received signal in the case of discrete multipath, given by *Equation (D.6)*, reduces to

$$d_l(t) = \sum_{i}^{L} \beta_i(t) e^{-j\vartheta_i(t)} \tag{D.11}$$

where $\theta_i(t) = 2\pi f_c \tau_i(t)$. Note that the subscript in *Chapter 4*, *Equation (4.12)* is dropped compared to *Equation (D.11)*, because all signals are assumed to be at baseband in *Chapters 1* to *7*. At time t, the received signal consists of the sum of a number of time-variant vectors (phasors) having amplitudes $\beta_i(t)$ and phases $\theta_i(t)$. Note that large dynamic changes in the medium are required for $\beta_i(t)$ to caused a significant change in the received signal. On the other hand, $\theta_i(t)$ will change by 2π rad whenever $\tau_i(t)$ changes by $1/f_c$. But $1/f_c$ is very small and, thus $\theta_i(t)$ can change by 2π rad with relatively small motions of the medium. As described in Appendix C, *Section C.2*, the random phases and amplitudes of

the received signal results in signal fading. The fading phenomenon is primarily a result of the time variations in the phases $\theta_i(t)$. That is, the randomly time-variant phases $\theta_i(t)$ associated with the vectors $\{\beta_i\, e^{-j\theta_i}\}$ at times result in the vectors adding destructively (see Appendix C, *Section C.2, Figure C.2*). When this occurs, the resultant received signal $d_l(t)$ is very small or practically zero. At other times, the vectors $\{\beta_i\, e^{-j\theta_i}\}$ add constructively, so that the received signal is large (see *Figure C.2*). Thus, the amplitude variations in the received signal, termed signal fading, are due to the time-variant multipath characteristics of the channel.

The delays $\tau_i(t)$, associated with the different signal paths, will also change at different rates and in an unpredictable (random) manner. This implies that the received signal $d_l(t)$ in *Equation (D.11)* can be modelled as a random process that is usually assumed to be stationary.

D.4 CHANNEL CORRELATION FUNCTIONS AND POWER SPECTRA

It is necessary to develop correlation functions and power spectral density functions that define the characteristics of a fading multipath channel. This analysis can be made in the time domain as well as the frequency domain.

D.4.1 Time domain analysis

Assuming that the channel impulse response $c(\tau;t)$ is wide sense stationary and a complex-valued random process in the t variable, the autocorrelation function of $c(\tau;t)$ can be defined as in *Equation (D.12)*

$$\Phi_c(\tau_1, \tau_2; \Delta t) = \frac{1}{2} E\left[c^*(\tau_1; t)c(\tau_2; t + \Delta t)\right] \qquad \text{(D.12)}$$

In most radio transmission media, the attenuation and phase shift of the channel associated with path delay τ_1 is uncorrelated with the attenuation and phase shift associated with path

delay τ_2, which is called uncorrelated scattering. Thus, if an assumption is made that the scattering at two different delays is uncorrelated, *Equation (D.12)* can rewritten as

$$\frac{1}{2}E\left[c^*(\tau_1;t)c(\tau_2;t+\Delta t)\right]=\Phi_c(\tau_1;\Delta t)\delta(\tau_1-\tau_2) \qquad \text{(D.13)}$$

If $\Delta t = 0$ in *Equation (D.13)*, the resulting autocorrelation function $\Phi_c(\tau;0)\equiv\Phi_c(\tau)$ is simply the average power output of the channel as a function of the time delay τ. For this reason, $\Phi_c(\tau)$ is called the multipath intensity profile or the delay power spectrum of the channel. In general, $\Phi_c(\tau;\Delta t)$ gives the average power output as a function of the time delay τ and the difference Δt in observation time.

In practice, the function $\Phi_c(\tau;\Delta t)$ is measured by transmitting very narrow pulses or, equivalently, a wideband signal and cross-correlating the received signal with a delayed version of itself. Typically, the measured function $\Phi_c(\tau)$ may appear as shown in *Figure D.3*. The range of values of τ over which $\Phi_c(\tau)$ is essentially non-zero or above a certain threshold is called the RMS delay spread of the channel and is denoted by ϑ_τ (see *Chapter 4, Figure 4.2*).

D.4.2 Frequency domain analysis

In the frequency domain the characterization of the time-variant multipath channel can be accomplished by taking the Fourier transform of *c(τ;t)*. This results in a time-variant transfer function *C(f;t)*, where *f* is the frequency variable. Thus,

$$C(f;t)=\int_{-\infty}^{\infty}c(\tau;t)e^{-j2\pi f\tau}\,d\tau \qquad \text{(D.14)}$$

If *c(τ;t)* is modelled as a complex-valued zero-mean Gaussian random process in the *t* variable, it follows that *C(f; t)* also has the same statistics. Under the assumption that the

channel is wide-sense-stationary, the autocorrelation function in the frequency domain can be defined as

$$\Phi_C(f_1, f_2; \Delta t) = \frac{1}{2} E\left[C^*(f_1; t) C(f_2; t + \Delta t)\right] \qquad \text{(D.15)}$$

Since *C(f; t)* is the Fourier transform of *c(τ;t)*, the autocorrelation function $\Phi_C(f_1, f_2; \Delta t)$ is also related to $\Phi_c(\tau; \Delta t)$ by the Fourier transform. It was shown by Proakis [6] that substitution of *Equation (D.14)* into *Equation (D.15)* resulted in

$$\Phi_C(f_1, f_2; \Delta t) \equiv \Phi_C(\Delta f; \Delta t) \qquad \text{(D.16)}$$

where $\Delta f = f_2 - f_1$. From *Equation (D.16)* it is observed that the autocorrelation function of *C(f; t)* in frequency is a function of only the frequency difference $\Delta f = f_2 - f_1$. Accordingly $\Phi_C(\Delta f; \Delta t)$ is known as the spaced-frequency, spaced-time correlation function of the channel. It can be measured in practice by transmitting a pair of sinusoids separated by Δf and cross-correlating the two separately received signals with a relative delay Δt.

D.4.3 Relationship between the frequency and time domain

Time delays in the channel

If $\Delta t = 0$ in *Equation (D.16)*, $\Phi_C(\Delta f; 0) \equiv \Phi_C(\Delta f)$ and $\Phi_c(\tau; 0) \equiv \Phi_c(\Delta \tau)$, the Fourier transform relationship is

$$\Phi_C(\Delta f) = \int_{-\infty}^{\infty} \Phi_c(\tau) e^{-j2\pi\Delta f \tau} d\tau \qquad \text{(D.17)}$$

The relationship is shown graphically in *Figure D.3*. Since $\Phi_C(\Delta f)$ is an autocorrelation function in the frequency variable, it provides a measure of the channel's frequency coherence. As a result of the Fourier transform relationship between $\Phi_C(\Delta f)$ and $\Phi_c(\tau)$,

the reciprocal of the RMS delay spread ϑ_τ is a measure of the coherence bandwidth of the channel. That is,

$$BW_c \approx \frac{1}{\vartheta_\tau} \tag{D.18}$$

where BW_c denotes the coherence bandwidth as defined in Appendix C. The coherence bandwidth is a measure of the frequency separation of two tones that will still be correlated. If the frequency separation between the two tones were larger than the coherence bandwidth, the channel affects the tones differently. Thus, if the bandwidth of an information-bearing signal is greater than the coherence bandwidth of the channel, the channel is said to be frequency selective. In this case the signal is severely distorted. If the bandwidth of the information-bearing signal is small in comparison to the coherence bandwidth of the channel, the channel is said to be non-frequency selective.

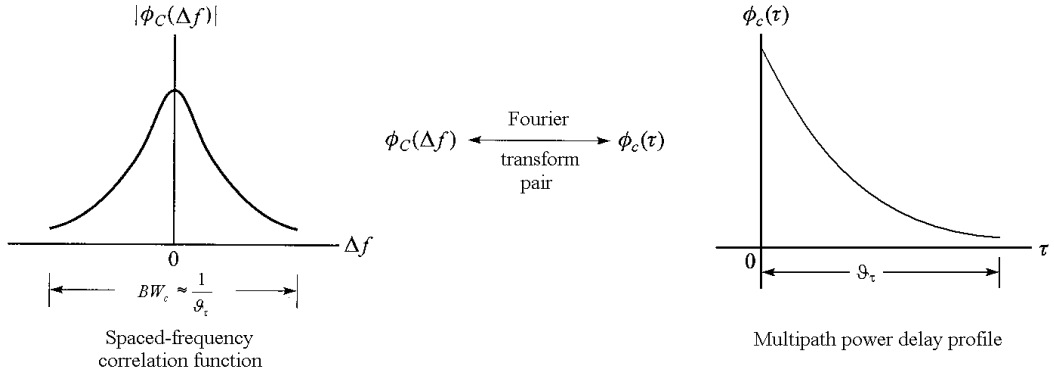

Figure D.3. Graphical relationship between $\Phi_C(\Delta f)$ and $\Phi_c(\tau)$, taken from Proakis, pp. 806 [6].

Time variations in the channel

Time variations in the channel are measured by the parameter Δt in $\Phi_C(\Delta f;\Delta t)$ and cause Doppler spreading of the signals. To relate the Doppler effects to the time variations of the channel, a function $S_c(\Delta f;f)$ is defined as the Fourier transform of $\Phi_C(\Delta f;\Delta t)$ with respect to the variable Δt. Thus,

$$S_C(\Delta f;\ f) = \int_{-\infty}^{\infty} \Phi_C(\Delta f;\Delta t) e^{-j2\pi f \Delta t} d\Delta t \qquad \text{(D.19)}$$

If Δf is set to zero, representing a single frequency tone, $S_C(0;f) \equiv S_C(f)$, and *Equation (D.19)* becomes

$$S_C(f) = \int_{-\infty}^{\infty} \Phi_C(0;\Delta t) e^{-j2\pi f \Delta t} d\Delta t \qquad \text{(D.20)}$$

$S_c(f)$ is a power spectrum that relates the signal intensity to the Doppler frequency f_d. Hence, $S_c(f)$ is called the Doppler power spectrum of the channel. If the channel is time-invariant, that is $\Phi_C(0;\Delta t) = 1$, *Equation (D.20)* reduces to the delta function, $S_c(f) = \delta(f)$. Therefore, when the channel is time-invariant, no spectral broadening is observed in the transmission of a single frequency tone.

The range of values over which $S_c(f)$ is essentially non-zero, is called the Doppler spread BW_d of the channel. Following the same argument as in the previous section, the Doppler power spectrum $S_c(f)$ is related to $\Phi_C(\Delta t)$ by the Fourier transform. Thus, the reciprocal of BW_d is a measure of the coherence time of the channel, given by

$$T_c \approx \frac{1}{BW_d} \qquad \text{(D.21)}$$

Thus, the coherence time is a time separation that will not cause any amplitude distortion in the signal. A slowly changing channel has a large coherence time, or equivalently a small Doppler spread, and visa versa. The graphical relationship between $S_c(f)$ and $\Phi_C(\Delta t)$ is shown in *Figure D.4*.

Another Fourier transform relationship exists between $\Phi_c(\tau;\Delta t)$ and $S_C(\Delta f;f)$
This relationship was derived by Proakis [6] and is denoted as

$$S(\tau;\ f_d) = \int_{-\infty}^{\infty}\int_{-\infty}^{\infty} \Phi_C(\Delta f;\Delta t) e^{-j2\pi f_d \Delta t} e^{j2\pi\tau\Delta f} d\Delta t d\Delta f \qquad \text{(D.22)}$$

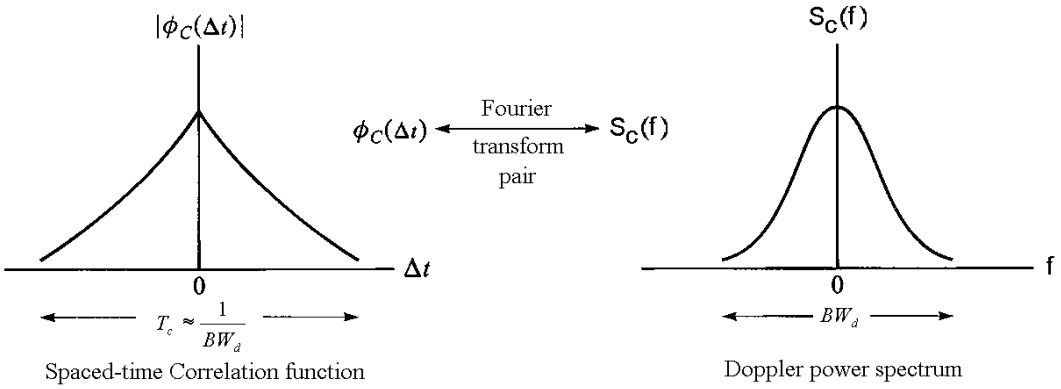

Figure D.4. Graphical relationship between $\Phi_C(\Delta t)$ and $S_C(\lambda)$, taken from Proakis, pp. 807 [6].

The function $S(\tau; f)$ is called the scattering function of the channel. The scattering function provides a statistical measure of the output power of the channel, expressed as a function of the time delay τ and the Doppler frequency f_d.

In *Section D.4*, a rough approximation was derived for the delay spread due to multipath. This was merely presented to show the graphical representation between the coherence bandwidth and delay spread, as well as the coherence time and Doppler spread. In *Sections D.5* and *D.6* more accurate approximations [1, 5, 7] are derived for the delay - and Doppler spread.

D.5 DELAY SPREAD

As stated in the previous section, if $\Delta t = 0$ in *Equation (D.13)*, $\Phi_c(\tau;0) \equiv \Phi_c(\Delta\tau)$ which is the multipath power delay profile. The multipath power delay profile may also be defined in terms of the scattering function $S(\tau; f)$, given in *Equation (D.22)*, by averaging it over all Doppler shifts f_d. That is,

$$\Phi_c(\tau) = \int_{-f_d}^{f_d} S(\tau; f)df \qquad \text{(D.23)}$$

Figure D.5 shows an example of a delay power spectrum that depicts a typical plot of the power spectral density versus the received time delays relative to shortest echo path. The

"threshold level" included in *Figure D.5* defines the power level below which the receiver fails to operate satisfactorily. Expanding on *Chapter 4*, *Section 4.2*, where only delay spread was defined, the terms excess delay, average delay and RMS delay spread are defined here. In order to do so, two statistical moments of $\Phi_c(\tau)$ are of interest, the average delay, τ_{av}, and the RMS delay spread, ϑ_τ (see *Figure D.5*). Note that the RMS delay spread defined here is the same as the delay spread defined in *Chapter 4*, *Section 4.7*. Also note that *Figure D.5* is a multipath power delay profile for an outdoor environment, where *Figure 4.2* in *Chapter* 4 is a typical indoor multipath power delay profile.

The average delay is defined as the first central moment (i.e., the mean) of $\Phi_c(\tau)$, shown by

$$\tau_{av} = \frac{\int_0^\infty \tau \Phi_c(\tau) d\tau}{\int_0^\infty \Phi_c(\tau) d\tau} \tag{D.24}$$

The RMS delay spread is defined as the root square of the second central moment of $\Phi_c(\tau)$, as shown by

$$\sigma_\tau = \left(\frac{\int_0^\infty (\tau - \tau_{av})^2 \Phi_c(\tau) d\tau}{\int_0^\infty \Phi_c(\tau) d\tau} \right)^{1/2} \tag{D.25}$$

As stated in *Section D.4* and given in *Equation (D.18)*, the reciprocal of the RMS delay spread ϑ_τ is a measure of the coherence bandwidth, BW_d, of the channel.

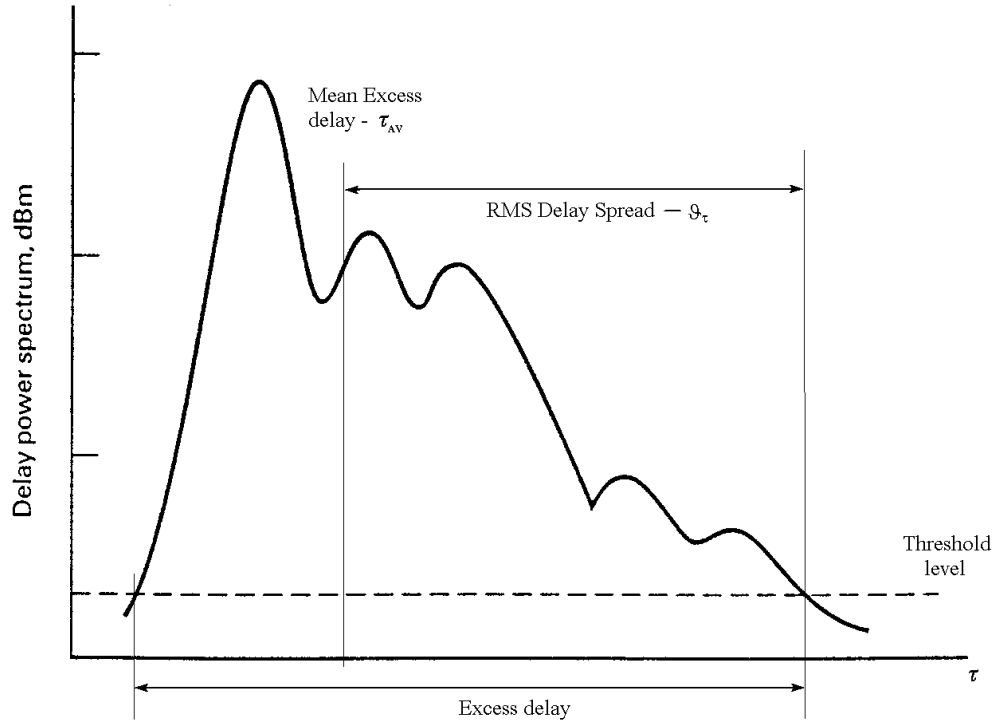

Figure D.5 The multipath power delay profile for a mobile radio channel, showing τ_{av} and ϑ_τ. Partially taken from Haykin [7].

D.5.1 Delay spread bound

Assuming that the longest propagation delay (excess delay, as shown in *Figure D.5*) between a base station and a mobile is $\tau_{max,}$ and that reflection coefficients are 100% uncorrelated, Feher [5] derived an upper bound to be

$$\tau_{\max} = \frac{1}{4\pi}\frac{1}{f}\sqrt{\frac{P_T}{P_{R\min}}} \qquad \text{(D.26)}$$

where :

P_T is the transmitted power (in dBm),

P_{Rmin} is minimum received power required at the receiver (in dBm),

f is the frequency at which the communication link operates, and

τ_{max} is the maximum excess delay time.

Delay spread field measurements

Typical RMS delay spread field measurements, obtained from Feher [5], are as follow:

- Cellular Systems, for example GSM (coverage up to 10km, RMS delay spread up to 100 μs)
- Land-mobile radio (coverage up to 70km, RMS delay spread up to 350 μs)
- Indoor PCSs, for example WLANs (coverage up to 30m, RMS delay spread up to 300 ns)

D.6 DOPPLER SPREAD

As stated earlier, the Doppler power spectrum is given by *Equation (D.20)*. The Doppler power spectrum may also be defined in terms of the scattering function $S(\tau; f)$, by averaging it over all possible propagation delays, shown in *Equation (D.27)*.

$$S_C(f) = \int_{-\infty}^{\infty} S(\tau; f) d\tau \qquad \text{(D.27)}$$

Assuming that the Doppler shift f_d may have positive and negative values with equal likelihood, the mean Doppler shift is therefore zero. The square root of the second moment of the Doppler spectrum is thus defined by

$$BW_d = \left(\frac{\int_0^{f_d} (f)^2 S_C(f) df}{\int_0^{f_d} S_C(f) df} \right)^{1/2} \qquad \text{(D.28)}$$

The parameter BW_d provides a measure of the width of the Doppler power spectrum, as shown in *Figure D.5*. Some typical values encountered in a mobile radio environment for Doppler spread, due to motion of a vehicle, ranges between 10 Hz to 200 Hz.

D.6.1 Doppler power spectrum for mobile radio channels

A widely used model for the Doppler power spectrum of mobile radio channels is the so-called Jakes's model [74]. In this model the autocorrelation, $\Phi_C(\Delta t)$ of the time-variant transfer function *C(f ; t)* from *Equation (D.15)* is given as

$$\begin{aligned}\Phi_C(\Delta t) &= \frac{1}{2}E\left[C^*(f;t)C(f;t+\Delta t)\right] \\ &= I_0\left(2\pi f_d \Delta t\right)\end{aligned} \tag{D.29}$$

where $I_0(\bullet)$ is the zero-order Bessel function of the first kind and f_d is the Doppler frequency as defined in *Equation (D.2).*

The Fourier transform of $\Phi_C(\Delta t)$, as shown in *Section D.4.3,* yields the Doppler power spectrum at baseband. That is

$$\begin{aligned}S_C(f) &= \int_{-\infty}^{\infty} \Phi_C(\Delta t) e^{-j2\pi f \Delta t} d\Delta t \\ &= \int_{-\infty}^{\infty} I_0\left(2\pi f_d \Delta t\right) e^{-j2\pi f \Delta t} d\Delta t \\ &= \begin{cases} \dfrac{1}{\pi f_d} \dfrac{1}{\sqrt{1-(f/f_d)^2}} & (|f| \le f_d) \\ 0 & (|f| \le f_d) \end{cases}\end{aligned} \tag{D.30}$$

The plot of $S_C(f)$ is shown in Appendix C, *Section C.3.3, Figure C.3.*

D.7 FADING CHANNEL SIMULATOR MODEL

In order to obtain Rayleigh and Rician statistical distributions, as described in Chapter 4, Clarke's model [75] can be used.

D.7.1 Description of the fading channel simulator

Clarke's fading simulator (*Figure D.6*) consists of two orthogonal independent Gauss noise sources with zero mean and unit variance in each branch, followed by a Doppler shaping filter. To simulate both a Rayleigh, as well as a Rician fading, a Rician factor is added to the in-phase branch (note that the fading is Rayleigh distributed when $K = -\infty$). The input signal is divided into an in-phase $S_I(t)$ branch and quadrature branch $S_Q(t)$. The quadrature branch is formed by applying the Hilbert transform to the input signal, which is only a 90-degrees phase shift from the in-phase signal frequency. The in-phase and quadrature branches are then respectively multiplied by the fading spectrum branches $n_I(t)$ and $n_Q(t)$ to produce $f_I(t)$and $f_Q(t)$. These two branches are added together and scaled by the C_{SCALE} constant to produce an output signal that has the same power as the input signal. The output signal $d(t)$ is a Rayleigh/Rician fading signal, depending on the Rician constant, which exhibits the proper Doppler spread and time correlation introduced in the channel.

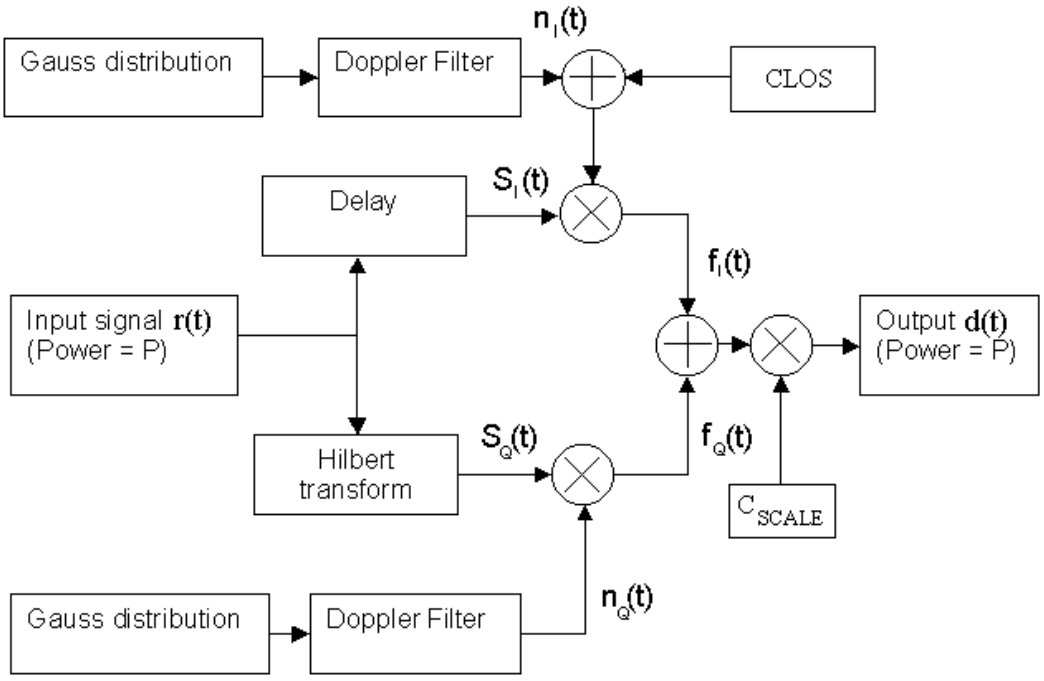

Figure D.6 Clarke's model for a fade simulator employing both Rayleigh and Rice fading.

D.7.2 Derivation of the *CLOS* and C_{SCALE} constants

From *Figure D.6* the in-phase branch is equal to

$$f_I(t) = S_I(t)\left[n_I(t) + (CLOS)\right] \tag{D.37}$$

and the quadrature branch is equal to

$$f_Q(t) = S_Q(t)\left[n_Q(t)\right] \tag{D.38}$$

The output of the fading simulator is therefore equal to

$$d(t) = C_{SCALE}\left[f_I(t) + f_Q(t)\right] \tag{D.39}$$

Substitution of *Equations (D.37)* and *(D.38)* into *Equation (D.39)* yields

$$d(t) = C_{SCALE}\left[S_I(t)n_I(t) + S_I(t)(CLOS) + S_Q(t)n_Q(t)\right] \tag{D.40}$$

Equation (D.40) can be rewritten in a form that consists of the LOS and NLOS part, that is

$$d(t) = C_{SCALE}\left[\underbrace{S_I(t)(CLOS)}_{LOS} + \underbrace{S_I(t)n_I(t) + S_Q(t)n_Q(t)}_{NLOS}\right] \tag{D.41}$$

The Rician constant K is defined as the ratio between the LOS signal component and the signal scatter components (NLOS). Thus

$$K = 10\log_{10}\left[\frac{\sigma^2{}_{LOS}}{\sigma^2{}_{NLOS}}\right] \tag{D.42}$$

If the input signal power is denoted by P, the power of the signal can be written as

$$\sigma^2{}_{u(t)} = E\left[u^2(t)\right] = P \tag{D.43}$$

The power in the in-phase and quadrature branches also equals *P*, respectively, because the Hilbert transform only produces a 90 degrees phase shift of the input signal. Thus the quadrature branch is a 90-degrees phase shift from the in-phase signal.

$$E\left[S_I{}^2(t)\right] = E\left[S_Q{}^2(t)\right] = P \tag{D.44}$$

From *Equation (D.41)*, the LOS and NLOS components of *r(t)* is

$$\begin{aligned} LOS &= S_I(t)(CLOS) \\ NLOS &= S_I(t)n_I(t) + S_Q(t)n_Q(t) \end{aligned} \tag{D.45}$$

Thus, the power of the LOS signal path is

$$\begin{aligned} \sigma^2{}_{LOS} &= E\left[LOS^2\right] = E\left[(CLOS)^2 S_I{}^2(t)\right] \\ &= (CLOS)^2 E\left[S_I{}^2(t)\right] \\ &= (CLOS)^2 P \end{aligned} \tag{D.46}$$

The power of the NLOS or scatter component of the signal is

$$\begin{aligned} \sigma^2{}_{NLOS} &= E\left[NLOS^2\right] = E\left[\left(S_I(t)n_I(t) + S_Q(t)n_Q(t)\right)^2\right] \\ &= E\left[S_I{}^2(t)n_I{}^2(t) + 2S_I(t)n_I(t)S_Q(t)n_Q(t) + S_Q{}^2(t)n_Q{}^2(t)\right] \\ &= E\left[S_I{}^2(t)n_I{}^2(t)\right] + 2E\left[S_I(t)n_I(t)S_Q(t)n_Q(t)\right] + E\left[S_Q{}^2(t)n_Q{}^2(t)\right] \\ &= E\left[S_I{}^2(t)\right]E\left[n_I{}^2(t)\right] + 2E\left[S_I(t)\right]E\left[n_I(t)\right]E\left[S_Q(t)\right]E\left[n_Q(t)\right] + E\left[S_Q{}^2(t)\right]E\left[n_Q{}^2(t)\right] \end{aligned} \tag{D.47}$$

But, $E\left[n_I{}^2(t)\right]$ and $E\left[n_Q^2(t)\right]$ is the variance of a Gauss distribution after Doppler filtering, thus

$$E\left[n_I{}^2(t)\right] = E\left[n_Q{}^2(t)\right] = 1 \tag{D.48}$$

and $E\left[n_I(t)\right]$ and $E\left[n_Q(t)\right]$ is the mean of a Gauss distribution, thus

$$E\left[n_I(t)\right] = E\left[n_Q(t)\right] = 0 \tag{D.49}$$

Using *Equation (D.48)* and *(D.49)*, *Equation (D.47)* reduces to

$$\begin{aligned}\sigma^2{}_{NLOS} &= E\left[S_I{}^2(t)\right] + E\left[S_Q{}^2(t)\right] \\ &= 2P\end{aligned} \tag{D.50}$$

Thus, from *Equation (D.46)* and *(D.50)*

$$\frac{\sigma^2{}_{LOS}}{\sigma^2{}_{NLOS}} = \frac{E\left[LOS^2\right]}{E\left[NLOS^2\right]} \tag{D.51a}$$

$$= \frac{(CLOS)^2 P}{2P} \tag{D.51b}$$

Substituting *Equation (D.51b)* into *Equation (D.42)*, the Rician factor, *CLOS*, can be written in terms of the Rician constant *K*, thus

$$CLOS = 10\log_{10}\left[\sqrt{2K}\right] \tag{D.52a}$$

in dB form and

$$CLOS = \sqrt{2K} \tag{D.52b}$$

in linear form. For unity power gain through the fading simulator, the following condition must be met:

$$P_{in} = P_{out} = P \tag{D.53}$$

Equation (D.53) states that the output power must be equal to the input power, which in this case is denoted by P (see *Figure D.6*). Thus:

$$\sigma^2{}_{u(t)} = \sigma^2{}_{d(t)}$$

$$E\left[u^2(t)\right] = E\left[d^2(t)\right]$$

But the input power is P, thus

$$P = E\left[d^2(t)\right]$$

$$= E\left[\left(C_{SCALE}\left[S_I(t)n_I(t) + S_I(t)(CLOS) + S_Q(t)n_Q(t)\right]\right)^2\right]$$

$$= E\left[(C_{SCALE})^2\left(S_I{}^2(t)(CLOS)^2 + (CLOS)S_I(t)n_I(t) + (CLOS)S_I(t)S_Q(t)n_Q(t) + \right.\right.$$

$$S_I{}^2(t)n_I{}^2(t) + (CLOS)S_I{}^2(t)n_I(t) + S_I(t)S_Q(t)n_I(t)n_Q(t) + S_Q{}^2(t)n_Q{}^2(t) +$$

$$\left.\left.(CLOS)S_I(t)S_Q(t)n_Q(t) + S_I(t)n_I(t)S_Q(t)n_Q(t)\right)\right] \qquad \text{(D.54)}$$

Using *Equations (D.48)* and *(D.49)*, *Equation (D.54)* reduces to

$$\mathrm{P} = (C_{SCALE})^2 E\left[S_I{}^2(t)(CLOS)^2 + S_I{}^2(t)n_I{}^2(t) + S_Q{}^2(t)n_Q(t)\right]$$

$$= (C_{SCALE})^2\left(E\left[S_I{}^2(t)(CLOS)^2\right] + E\left[S_I{}^2(t)n_I{}^2(t)\right] + E\left[S_Q{}^2(t)n_Q(t)\right]\right)$$

$$= (C_{SCALE})^2\left((CLOS)^2 E\left[S_I{}^2(t)\right] + E\left[S_I{}^2(t)\right]E\left[n_I{}^2(t)\right] + E\left[S_Q{}^2(t)\right]E\left[n_Q(t)\right]\right)$$

$$= (C_{SCALE})^2\left((CLOS)^2 P + P + P\right) \qquad \text{(D.55)}$$

Rewriting *Equation (D.55)* in terms of the Rician factor *CLOS* and the power P, yields

$$C_{SCALE} = \sqrt{\frac{P}{(CLOS)^2 P + 2P}}$$

$$C_{SCALE} = \sqrt{\frac{1}{CLOS^2 + 2}} \qquad \text{(D.56)}$$

and in terms of the Rician constant K:

$$C_{SCALE} = \frac{1}{\sqrt{2(1+K)}} \tag{D.57}$$